Master of Science Thesis in Electrical Engineering
Department of Electrical Engineering, Linköping University, 2018

Estimation of Engine Gas Temperatures During Pressure Transients

Marcus Wallson

Master of Science Thesis in Electrical Engineering

Estimation of Engine Gas Temperatures During Pressure Transients

Marcus Wallson

LiTH-ISY-EX--18/5145--SE

Supervisor: **Robin Holmbom**
ISY, Linköpings universitet
Samuel Alfredsson
Volvo Cars Corporation

Examiner: **Professor Lars Eriksson**
ISY, Linköpings universitet

Division of Vehicular Systems
Department of Electrical Engineering
Linköping University
SE-581 83 Linköping, Sweden

Abstract

Coming stringent regulatory emissions requirements with Real Driving Emissions testing amplifies the need for efficient engine control at all driving scenarios. This thesis has investigated the air-flow transients that appears when changing the throttle position very fast, such as at a stop sign. Available information about the intake manifold temperature is today mainly sensor-based or zero-dimensional. Since the temperature of the air affects the fuel controller(s) and is believed to be able to help the knock-controller as well, a more detailed description of the temperature is warranted. Three different one-dimensional interpretations of the intake manifold has been modeled and one of them is implemented in a full air-path simulation - from the throttle to the exhaust. The best suited simulation model is validated against measurement data and compared to the well know adiabatic control volume model, which is zero-dimensional. The effect on the temperature contributed by the VVT, turbo, throttle-settings and engine speed was tested in a test cell. The results shows that the computational efficiency varies between the different one-dimensional intake manifold models and that one-dimensional accuracy comes at a great cost of computational power. The testing and validation showed that the pressure difference and throttle ramping time had a big impact and that the positive transients are more predictable with current models, compared to the negative transients.

Acknowledgments

First and foremost would I like to thank Volvo Cars for the opportunity to work with this thesis. The team at Volvo has supported this thesis, and its sister theses, with great passion. I would especially like to thank Samuel Alfredsson, my supervisor at Volvo, for thorough and fast responses when I was in doubt and great constructive discussions.

I would also like give a big thanks to all personnel at Fordonssystem who have been very helpful. A special thanks is well-deserved to the following individuals: firstly, Robin Holmbom, my supervisor, for all valuable input and interesting discussions. Secondly, Tobias Lindell for helping me when installing the temperature sensors and making the testing run smoothly. Thirdly, Lars Eriksson for giving a solid theoretical foundation in his courses and depth with his published articles and books.

Lastly I would like to thank my family and friends for the love and support.

Linköping, May 2018
Marcus Wallson

Contents

Notation **ix**

1 Introduction **1**
1.1 Background . . . 1
1.2 Problem Formulation . . . 1
1.3 Purpose and Goal . . . 2
1.4 Outline . . . 2

2 System Introduction **5**
2.1 System Overview . . . 5
2.2 Four-stroke SI-engine . . . 7
2.3 Explanation to Expressions . . . 7

3 Related Research **9**
3.1 Knock- & A/F-control . . . 9
3.2 Intake Manifold Fluid Dynamics . . . 10
3.3 Residual gases & EGR . . . 11
3.4 Pulsating Flow . . . 12

4 Theory & Modeling **13**
4.1 Intake Manifold Fluid Dynamics . . . 13
4.1.1 Staggered Grid . . . 13
4.1.2 Courant-Friedricks-Lewy Criterion (CFL) . . . 19
4.1.3 Adiabatic Intake Manifold . . . 19
4.2 Heat Transfer . . . 19
4.2.1 Convection and Conduction . . . 19
4.3 Cylinder and Combustion Modeling . . . 20
4.3.1 In Cylinder Single-Zone Model . . . 20
4.3.2 Net Heat Release . . . 21
4.3.3 Thermodynamic Parameter Model . . . 23
4.3.4 Residual Gas . . . 24
4.3.5 Cylinder Geometry . . . 24
4.4 Compressible Flow Model . . . 25

4.5 Valve Mechanics 25

5 Test Setup **31**
5.1 Data Sampling 32
5.2 Temperature Sensor Placement 32
5.3 Pegging the Cylinder Pressure 33
5.4 Tests 33

6 Results **35**
6.1 Simulation Setup 35
6.1.1 Control Volume Setup 35
6.1.2 Simulation comparison between *'Method 1', 'Method 2'* & *'Method 3'* 36
6.1.3 Temperature and Time-step Correlation 37
6.2 Full Model Simulation 38
6.2.1 Temperature Transient Validation 39
6.2.2 Temperature Transient Correlation with in-cylinder Temperature 41
6.3 Test Data Results 44
6.3.1 Pressure Gradient & Engine Speed 44
6.3.2 Negative Transient Phenomena 49
6.3.3 VVT-settings 49
6.3.4 Turbo-boosted Pressure Transient 50
6.4 Sensitivity Analysis 50

7 Discussion **57**
7.1 Simulation Models 57
7.1.1 Model Choice 57
7.1.2 Control Volume Setup 58
7.1.3 Non-intake manifold model Accuracy Requirements 59
7.2 Intake Temperature Model Simplification 60
7.3 Measurement uncertainties 61

8 Conclusions & Future Work **63**
8.1 Conclusions 63
8.2 Future Work 64

A Test list **67**

Bibliography **73**

Notation

Abbreviations

Abbreviation	Desciption
VCC	Volvo Car Corporation
LiU	Linköpings universitet
ICE	Internal Combustion Engine
RPM	Revolutions Per Minute
CFD	Computational Fluid Dynamics
VVT	Variable Valve Timing
CA	Crank Angle
EGR	Exhaust Gas Recirculation
TDC	Top Dead Center
BTDC	Before Top Dead Center
ATDC	After Top Dead Center
BDC	Bottom Dead Center
MVEM	Mean Value Engine Model
SI-ENGINE	Spark Ignition Engine
IVC	Intake Valve Closing
IVO	Intake Valve Opening
EVC	Exhaust Valve Closing
EVO	Exhaust Valve Opening
MFB	Mass Fraction Burned
SBF	Spatial Basis Function
RMSE	Root Mean Squared Error

Variables

Notation	Desciption
T	Temperature
m	Mass
ρ	Density
u	Velocity
e	Specific internal energy
h	Specific enthaply
A	Cross-sectional area
$\dot{q}$	Specific rate of heat transfer
p	Pressure
C_d	Discharge coefficient
c_v	Specific heat constant volume
c_p	Specific heat constant pressure
V	Volume
R	Ideal gas constant
ϵ	Diffusion coefficient
γ	Specific heat ratio
W	Work
Q_{hr}	Heat release
Q_{ht}	Heat transfer
$(A/F)_s$	Stoichiometric air-fuel ratio

1

Introduction

This chapter provides the reader with a short problem formulation, the goals and purpose, expected results and an outline of this Master Thesis.

1.1 Background

The goal with developing modern turbocharged SI-ENGINE is to deliver sufficient driveability with low fuel consumption and low emissions. Current knock-controllers are very restrictive and A/F-controllers lack information about the transient intake manifold temperature. This ”transient temperature” is most prominent when the driver steps on the gas when driving slowly, which is due to big pressure changes in the manifold. Coming stringent regulatory emissions requirements with difficult Real Driving Emission (RDE) tests magnifies the requirements on engine control and thus further model developments are a must.

1.2 Problem Formulation

The intake manifold temperature is dependent on several different factors e.g. residual gas, throttle mass flow, cylinder air-charge, LP-EGR, boost pressure, ambient temperature, heat transfer with surrounding engine temperature and intake valves, engine related pulsations, intake/exhaust valve control and water injection. The fastest transient temperatures are however mostly dependent on the pressure gradients caused by mass flow differences which occurs when the drives steps on the gas during low RPM. Furthermore, the transient intake manifold temperature affects the transient A/F-ratio and the engine’s knock-conditions which directly controls the efficiency of the combustion cycle. An improved and on-line feasible transient model would have the potential to improve the engine opera-

tion as well as decrease Research & Development cost. The model would provide additional information for the A/F-ratio controller and knock controller. Which ideally means that the engine would operate closer to minimum emissions since a decreased amount of unburnt fuel & knock decreases unwanted emissions. The Research & Development cost would decrease since it would e.g. reduce the mapping requirements for the engine knock control. Hence the transient temperature is dependent on many factors, both controllable and independent factors, and affects the engine's A/F-ratio control and knock-control further investigation is warranted.

1.3 Purpose and Goal

The main objective of this thesis is to define temperature models during transients, both in the intake manifold and the temperature in the cylinder at IVC. The simulation model aims to be able to predict the gradually increasing intake manifold temperature in the flow-direction. The model shall be derived from physically based equations and validated with previously stated contributing factors' physical states from measurement data. Measurement data will be received from several fast thermocouples placed inside the test cell and other available sensor data (clarified in Section 5). Developed simulation results shall be studied and used, in conjunction with measurement data, to suggest ways to simplify the models and in what areas finer models would pay off.

Expected results are clear plots showing the experimental transient temperature compared to simulated temperature at corresponding reference points. The simulation model should be able to simulate the entire air-path, from throttle to exhaust. The effects of VVT- and Turbo control on the transient temperature shall be presented and analyzed.

1.4 Outline

Description of the thesis' main chapters:

- **Chapter 1 – Introduction**
  Problem formulation, purpose and goal and expected results.

- **Chapter 2 – System Introduction**
  Introduction to the system; background information about the internal combustion engine and relevant available sensors on a production vehicle and the test cell.

- **Chapter 3 – Related Research**
  Review of current state of research in relevant areas.

- **Chapter 4 – Theory & Modeling**
  Relevant theory and models used in the thesis.

- **Chapter 5 – Test setup**
  Information regarding the test cell and experiment setup.
- **Chapter 6 – Results**
  Presents the results.
- **Chapter 7 – Discussion**
  Discussion regarding the results.
- **Chapter 8 – Conclusions & Future Work**
  Summation and suggestions on future work.

2

System Introduction

Introduction to the system; background information about the internal combustion engine and relevant available sensors on a production vehicle and the test cell.

2.1 System Overview

An SI-ENGINE is in a simplified manner illustrated in Figure 2.1 which shows that it has a throttle, an intake and exhaust manifold connected to an arbitrary amount of cylinders. The torque produced by the engine is dependent on a lot of factors but the main contributor is the amount of air and fuel of which is combusted. The amount of air added to the cylinder is mainly dependent on the pressure difference between the pressure inside the cylinder and the pressure in the intake manifold, this is further explained in Section 4.4. The focus is therefore on inducing a pressure change and studying the temperature effect. On a real engine this changed intake pressure is mainly controlled with the throttle. The test cell is a modified Volvo petrol engine. This means that it is driven on gasoline, direct injected, turbocharged and has a total cylinder volume of 2 liters across four cylinders. It is modified with several additional sensors mounted across the engine. Figure 2.1 shows where some of the sensors are mounted.

- Pressure sensors
    1. Intake manifold
    2. Exhaust manifold (additional)
    3. Cylinder (additional)
- Temperature sensors

1. Before throttle
2. Intake manifold
3. Exhaust manifold

- Mass flow sensor
  1. After air filter
- Lambda sensors
  1. Before and after the catalyst
- Tachometer
  1. Crank axle
- Position sensors
  1. Intake and exhaust camshaft positions (VVT-settings)
  2. Throttle position
  3. Wastegate position

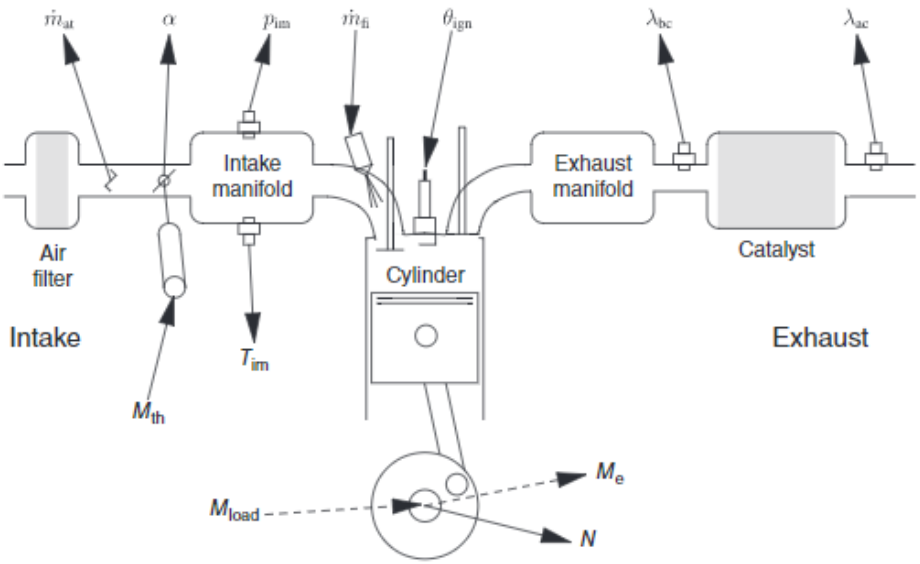

Figure 2.1: *Shows some of the available sensors. The picture does not include all components that are installed on the test engine, e.g. a compressor and an intercooler should be included between the throttle and air filter. The Figure is reproduced with permission from Eriksson and Nielsen (2014) Figure 7.1.*

2.2 Four-stroke SI-engine

The four stroke engine completes its cycle in two revolutions. These revolutions consists of four strokes; *Intake*, *Compression*, *Expansion* and *Exhaust*, see Figure 2.2. The first stroke is *Intake* which generally is defined as the motion from TDC to BDC. During this phase air is led through the inlet valves and into the cylinder. The next stroke is *Compression* which is the motion from BDC to TDC, during this phase fuel is injected, compressed and ignited. The next stroke is the *expansion* phase, during this phase the combustion energy expands the cylinder volume and therefore delivers positive torque to the crank shaft. The last phase is the *exhaust* phase, which tries to empty the cylinder of all exhaust gases. Some exhaust gases are left inside the cylinder and the cylinder pressure is very close to exhaust pressure. The cycle is completed at TDC and the cycle starts over with the *intake*-stroke. The cylinders can operate cycle-wise in pairs or individually, this design choice comes down to e.g the balancing of the engine and the amount of cylinders.

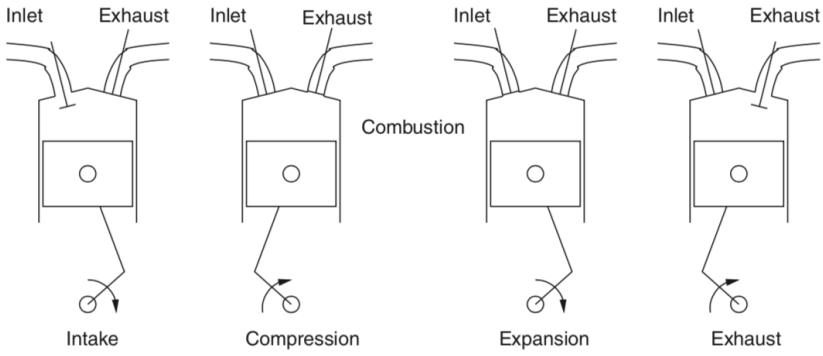

Figure 2.2: *Shows the four stroke operating cycle. The Figure is reproduced with permission from Eriksson and Nielsen (2014)*

2.3 Explanation to Expressions

Engine knock is when there occurs spontaneous ignition outside the flame propagation started by the controlled ignition by the spark plug. Figure 2.3 illustrates the knocking concept. Knocking causes a knocking sound and harmful vibrations that can destroy the engine (Heywood, 1988).
A/F-control stands for air-to-fuel ratio control, i.e. making sure that the injected amount of fuel matches, with the desired ratio, to the amount of added air.

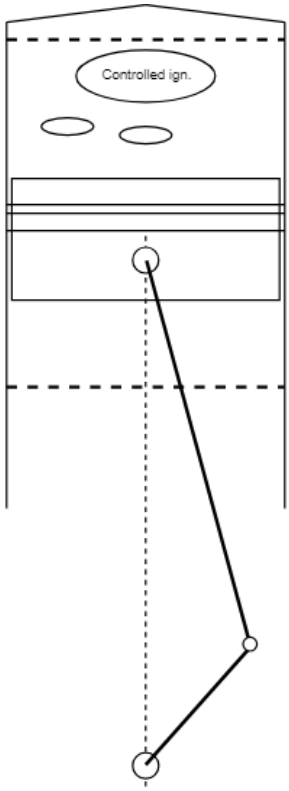

Figure 2.3: *Shows the cylinder and the combustion chamber. The circles outside the controlled ignition represents spontaneous combustions/knocking.*

3

Related Research

This chapter presents related research regarding the different effects that affects the intake manifold temperature and certain engine controls that are affected by the intake temperature.

3.1 Knock- & A/F-control

Early forms of current knock control strategies are declared in Ham et al. (1996). These strategies are based on determining an acceptable knocking intensity measured from the engine's available knock sensor. The acceptable knocking intensity is translated to a threshold ignition crank axle angle. The ignition angle is delayed if there is knock above the accepted knock intensity since it decreases the probability of knocking. The magnitude of the retardation is determined from the knocking intensity. After the ignition angle has been delayed it is slowly pushed backwards till knock occurs again. Transient knock control is expanded with measured engine map. A knock controller without measured engine maps would overcompensate the ignition retardation and therefore operate further away from combustion optimum (Baik and Chun, 1996; Eriksson, 1999). These kinds of algorithms are used since they are computationally effective. More advanced model based control strategies has been investigated in Siokos et al. (2017), where the Shell model developed by Haletad et al. (1975), and an empirical induction-time correlation model developed by Douaud and Eyzat (1978) was compared. The Shell model which yielded better experiment results, but is not feasible in an on-line implementation due to its required computational power. To the author's knowledge no knock-control algorithm utilize the transient temperature at IVC.

A/F-control usually estimates the cylinder air-charge from volumetric efficiency, intake manifold temperature/pressure, VVT-position, engine RPM and

exhaust temperate/pressure. Blomqvist et al. (2000) considers seven different A/F-controllers under "real-life" transient operations. The report concluded that a neural network approach yielded lower RMS-error (Root Mean Square-error) than standard adapted-ECU algorithms during fast transients. The standard adapted-ECU algorithm performed better during slower transients. Ichiyanagi and Suzuki (2015) implemented and experimentally validated two feed-forward controllers which considers the heat transfer in the intake manifold. They used lumped heat transfer models based on previous work made in Izumi et al. (2007). The controllers were compared to a control algorithm based on a steady state engine-map, and the transient A/F fluctuation were decreased by an estimated 84 %.

3.2 Intake Manifold Fluid Dynamics

The intake manifold fluid being a compressible fluid means that the dynamics are very complex. Heywood (1988) presents filling and emptying models derived from the mass and energy conservation equations coupled with the mass flow rates in and out of the model – which in most cases means that the model is dependent on a volumetric efficiency map. He also presents a more advanced one-dimensional gas dynamic model which also captures the spatial dynamics. Other air-charge estimation methods using a cylinder pressure sensor are summarized in Eriksson and Thomasson (2017). The modern approach is to analyze it using CFD. CFD captures the fluid state changes as temperature and pressure in respect of the fluid dynamics as well as heat exchanges with the surroundings. Cheng et al. (1991) analyzed the intake manifold temperature and the in-cylinder HC concentration on a port-injected SI-engine during constant engine RPM and varying stationary throttle positions. Measured temperature dynamics showed that the temperature gradually increased with a decreased distance to the intake ports, big transients occurred mainly at IVO and IVC. The temperature transients increased with inlet pressure. The fraction of burnt gas during intake appeared to be successfully modelled as a function of inlet pressure (with no regard to VVT). Steady-flow operation CFD-calculations was made in Befrui (1994) which acted as a validation of CFD-simulations as an engineering tool. A few years later Bauer and Heywood (1996) investigated the transient gas temperature using CFD-calculations and experiment measurements. They focused on the intake manifold temperature gradient, backflow – which is exhaust gas flow into the intake manifold at IVO, and the displacement backflow – which is exhaust gas flow into the intake manifold due to inlet valve closing timing, i.e. depending on how early/late you close the inlet valve. Their investigation yielded similar results in both simulations and experiments and a linear regression (with manual fitting coefficients) for the temperature gradient. An anomaly temperature transient was detected when fresh air approached the intake valves, which the CFD-simulation did not predict. This temperature transient appeared even though the wall temperature was kept below the gas temperature. It also yielded similar heat transfer coefficient as other heat transfer researchers e.g. Zapf or Dittus-Boelter correla-

tion (Kakac et al., 1987; Zapf, 1969).

Bauer et al. (1997) modeled the valve and intake manifold wall heat transfers using experimental data for time-resolved heat flux and gas temperatures in and around the intake ports on a port-injected SI-engine. A one-dimensional model predicting the gas temperature was also presented. The derivation was based on the mass- and energy balances in the intake ports and the assumption of inlet pressure being constant during the intake process, i.e. assumed infinite pressure propagation speed. Heat transfer due to pulsations (pressure waves) was not included. Discretization was partly explicit with a leap-frog scheme (Bauer et al. (1997) refers to Strikwerda (1989)) and partly implicit during the diffusive part using the Crank-Nicolson method (Crank and Nicolson, 1996 (original: 1947)). The models include terms for the port-injections, which means that a direct-injection engine has to remove those terms but might be sufficient if water-injection is to be considered. Courant et al. (1928) presented a criterion necessary to fulfill when simulating these types of dynamics (partial differential equations) when integrating in explicit time schemes.

Renberg (2008) compared 1D- & 3D-simulation with CFD-simulations. The entire engine, with appropriate assumptions, is presented as one-dimensional equations. Regardless if 1D-simulations or CFD/3D-simulations were done similar results were yielded for the pressure gradient. Deviations appeared in pipe bends, where the one-dimensional simulations gave higher pressure gradients than three-dimensional simulations. A shortcoming of this report is that no empirical data from a test rig was used to validate the results.

An effective way for computing 3D-simulations, using an "Unconstructed Parallel Solver", are described in Bohbot et al. (2003); Zolver et al. (2003a,b). An extensive survey on 3D simulation simplification methods is presented in Hosain and Fdhila (2015). The survey presents methods to accelerate the computational time using hardware techniques as well as using advanced numerical methods. Hardware techniques utilizes parallel programming solely or on both the CPU and GPU. Advanced numerical methods can be mesh based, mesh free and hybrid methods, a typical "work-horse" method in Reduced Order Modelling (ROM) which uses the singular value decomposition. Combining several numerical methods can, for nonlinear heat conduction models reduce simulation times by 150 times (Astrid, 2004).

3.3 Residual gases & EGR

The residual gases, often called internal EGR, are the gases that gets trapped inside the combustion chamber or at the inlet ports (Heywood, 1988). The amount of residual gas that gets trapped depends on intake pressure and the intake and exhaust valve timings, i.e. it is dependent on the configured overlaps during the intake/exhaust strokes and the exhaust pressure. A model only using production-grade sensors is presented in Leroy et al. (2009). Eriksson and Nielsen (2014) considers the in-cylinder mixing as an adiabatic process. This means that the internal energy is unchanged, combined with an assumption of a constant heat

specific ratio would lead to a temperature at IVC being the weight-adjusted mean temperature, see Eq. (3.1).

$$T_{\text{IVC}} = \frac{m_r T_r + m_{af} T_{im}}{m_r + m_{af}} \tag{3.1}$$

If the engine has external EGR this adds another dimension to the air charge estimation, an inclusion method is presented in Eriksson and Nielsen (2014). An LP-EGR (Low pressure EGR) system would impact the temperature at IVC with lower exhaust gas temperature and therefore lower temperature gradient coupled to the residual gas.

3.4 Pulsating Flow

Since the fluid flow is pulsating, due to the nature of an ICE, makes it an interesting aspect to consider. There are two main types of pulsations, either pulsations induced by the cylinders' pumping strokes or if the ICE is turbocharged, which would transfer the predominant pulsating flow that occurs in the exhaust into the intake flow via the compressor. The effect of the pulsating flow on the heat transfer has been investigated by several researchers, but the conclusions are not uniform. Wang and Zhang (2005) simulates and validates experimentally a result which says that the heat transfer increases with pulsations, Shiibara et al. (2017) gets similar results when varying acceleration and deceleration for a water pipe. But Plotnikov and Zhilkin (2017) concludes that the local heat transfer is reduced by fluid unsteadiness.

4

Theory & Modeling

Presents the theory and models used in the thesis.

4.1 Intake Manifold Fluid Dynamics

As discussed in Section 3.2 the fluid dynamics can be simulated using advanced third party CFD-programs or using one- or three-dimensional simulations. This report will focus on making efficient but less detailed one-dimensional models since they will provide sufficient information for the application. Most one-dimensional models discretize or integrate the one dimensional governing differential equations. The discretization method leads to a grid of computational points where the governing equations are calculated, interpolations can be used between the points. The integration method leads to a finite amount of control volumes of which the states are calculated for.

4.1.1 Staggered Grid

Staggered grid is a one dimensional modeling method which divides the pipe into an arbitrary quantity of control volumes. These control volumes are assumed to be 'well-mixed' and therefore uses zero-dimensional equations to calculate each control volume's states. The combined data from all control volumes creates the one-dimensional model. The dynamics between the control volumes are decided by plug-modules which are placed between all control volumes, see Figure 4.1. The computations are done in a manner described in Figure 4.2. The computations needs to be fed a mass flow at both endpoints and the temperature of the mass flow. The mass flow originates, in this case, either from the throttle or from the intake valves. The control volume governing equations are thus using boundary conditions from a half time step before its time center and the plug

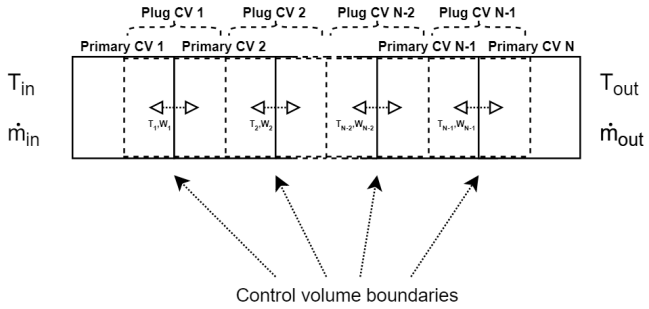

Figure 4.1: *Schematic view of the staggered grid modeling approach. The picture shows an arbitrary set of N control volumes, with a corresponding set of N-1 plug volumes. The interconnecting T:s and W:s represents the temperature of the flow and the mass flow between the control volumes. All volumes are spatially centered relative to each other.*

control volume are using state data from a half time step before its time center. This report considers three methods partly different modeling approaches to this staggered grid simulation setup. The first method (*'Method 1'*) is based on Öberg (2009), which uses the mass, energy and momentum balance equations as the governing equations. The medium is considered an ideal gas and the gas viscosity is neglected. The plug-module uses Newtons second law of motion to determine the dynamics between the control volumes, which means that the plug-volume does not consider any internal energy of the gas. The second method (*'Method 2'*) is based of Montenegro et al. (2011a,b) and is called 3DCell. This method uses the nonlinear Euler equations as the governing equations, the medium is considered an ideal gas and neglects the gas viscosity. This method differentiates itself from *Method 1* since it uses a time-centered (and spatially centered) difference grid that calculations made in the plug control volumes are made multiple time levels at the same time, this creates the opportunity of having second-order accuracy in time (Stockar et al., 2013). The third method Reduced Order Model (*'Method 3'*) is also based on the nonlinear Euler equations but separates itself from the two other methods as it can be implemented with an empirical link to the application.

Control Volume – Method 1 & 2

This method uses the mass and energy balance equations as the governing equations in the control volume. The pressure is approximated with the ideal gas law.

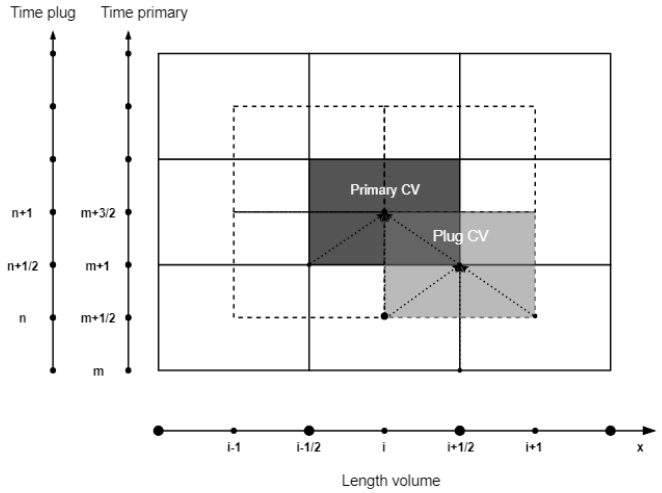

Figure 4.2: *Plot showing the staggered grid spatial and time steps.*

The governing equations in the control volume are

$$\begin{aligned} &\frac{\partial \rho}{\partial t} + \frac{\partial (\rho u)}{\partial x} + \frac{\rho u}{A}\frac{dA}{dx} = 0 \\ &\frac{\partial (\rho e_0)}{\partial t} + \frac{\partial (\rho u h_0)}{\partial x} + \frac{\rho u h_0}{A}\frac{dA}{dx} - \rho \dot{q} = 0 \end{aligned} \tag{4.1}$$

which is formulations of the mass and energy conservation laws. A case where the control volumes' volumes remains constant means that the third terms in both equations are redundant. This is the case for the intake manifold. The fluid is considered an ideal gas, i.e. the following equations:

$$p = \rho R T \qquad e = c_v(T)T \qquad h = c_p(T)T \tag{4.2}$$

where a common assumption is using constant specific heats.

Mass balance:

$$\left(\frac{dm_i}{dt}\right)_i^{m+1} = \dot{m}_{i-1/2}^{n+1/2} - \dot{m}_{i+1/2}^{n+1/2} \tag{4.3}$$

Energy balance:

$$\left(\frac{dE_i}{dt}\right)_i^{m+1} = \dot{H}_{i-1/2}^{n+1/2} - \dot{H}_{i+1/2}^{n+1/2} + \dot{Q}_i \tag{4.4}$$

Ideal gas law:

$$pV = mRT \Leftrightarrow p_i^{m+1} = \frac{m_i^{m+1} R T_i^{m+1}}{V_i} \tag{4.5}$$

The control volume states can either originate from up- or downstream. The input change in enthalpy ($\dot{H}_{in}$) is dependent on the upstream control volume states and the output change in enthalpy ($\dot{H}_{out}$) is dependent on the downstream

volume states. Eq. (4.6) presents how each enthalpy is calculated, which plug volume that is up or downstream depends on the flow direction.

$$\dot{H}_{i\pm1/2}^{n+1/2} = (T \cdot \dot{m} \cdot c_p(T))_{i\pm1/2} \tag{4.6}$$

The change in temperature is derived from the differentiation of the inner energy E=m · e where e = c_v(T) · T and is shown in Eq (4.7).

$$\frac{dT_i}{dt}^{m+1}_{i} = \frac{1}{m^{m+1} \cdot c_v(T)} \left(\frac{dE_i}{dt}^{m+1}_{i} - e(T)_i^m \frac{dm}{dt}^{m+1}_{i} \right) \tag{4.7}$$

Heat transfer ($\dot{Q}$), which is added in Eq. (4.4), is a subject that will be elaborated in Section 4.2.

Plug-volume – Method 1

This plug volume method is from Öberg (2009), which uses Newton's second law of motion with an ad-hoc dampening constant (k_{Fric}) to calculate the change of speed taking place between the control volumes, its function is shown in Eq. (4.8). The temperature and pressure of the flow is assumed to be unchanged from its originating control volume. The originating control volume is decided by the sign of the flow speed which is assumed to be as shown in Eq. (4.9). This will approximate the diffusion of the flow throughout the pipe.

$$\frac{du_{i+1/2}}{dt}^{n+1/2} = \frac{2A(p_i^{m+1/2} - p_{i+1}^{m+1/2})}{m_i^{m+1/2} + m_{i+1}^{m+1/2}} - u_{i+1/2}^n \cdot k_{Fric} \tag{4.8}$$

$$\begin{cases} T_{flow}^{n+1/2}, p_{flow}^{n+1/2} = T_i^{m+1/2}, p_i^{m+1/2} & \text{if u } > 0 \\ T_{flow}^{n+1/2}, p_{flow}^{n+1/2} = T_{i+1}^{m+1/2}, p_{i+1}^{m+1/2} & \text{if u } < 0 \end{cases} \tag{4.9}$$

The mass flow is calculated with the expression for mass flow and the ideal gas law.

$$\dot{m}_{i+1/2}^{n+1/2} = \frac{p_{flow}^{n+1/2} A u_i^{n+1/2}}{R T_{flow}^{n+1/2}} \tag{4.10}$$

Plug Volume – Method 2

The plug modelling is based on Montenegro et al. (2011a,b). Stockar et al. (2013) presents the approach used by them as well as an extension which increases the precision during subsonic flow. The starting point is the Euler momentum equation presented below.

$$\frac{\partial(\rho u)}{\partial t} + \frac{\partial(p + \rho u^2)}{\partial x} + \frac{\rho u^2}{A} \frac{dA}{dx} = 0 \tag{4.11}$$

The momentum equation is integrated over the plug volume using the following derivative

$$\frac{d\dot{m}_{i+1/2}}{dt}^{n+1/2} = \frac{1}{\Delta x}[(\rho u^2 + p)_{i+1}^{m+1/2} - (\rho u^2 + p)_i^{m+1/2}]A_{i+1/2} \tag{4.12}$$

and the enthalpy flow, which is used as an output in Stockar et al. (2013) is calculated with

$$\dot{H}_{i\pm1/2} = \dot{m}_{i\pm1/2} \cdot h_0 \tag{4.13}$$

where the direction of the flow directs what values to be used. The direction of the flow in the control volume is approximated with the sign of the mass flow, i.e. a negative mass flow changes the usually downstream position into the upstream position. The implementation done in this thesis calculates only the mass flows in the plug-volume and calculates the corresponding enthalpy flow in the control volume. This is done purely to create a modularity within the methods.

As a second-order solution does not guarantee stability for all solutions, especially for large pressure gradients an additional source/damping term is added to Eq. (4.12), which is shown in its entirety in Eq. (4.17) (Stockar et al., 2013). The source term is added to the Euler momentum equation as in Eq. (4.14).

$$\frac{\partial(\rho u A)}{\partial t} + \frac{\partial(\rho u^2 A + pA)}{\partial x} = \frac{\partial S}{\partial x} \tag{4.14}$$

The source term is defined in every control volume with differential equation defined in Eq. (4.15).

$$S = \varepsilon \frac{\partial(\rho u A)}{\partial x} \tag{4.15}$$

Where ε is defined by the following equation.

$$\varepsilon = \frac{u\Delta x}{2} - \frac{u^2 \Delta t}{2} \tag{4.16}$$

The resulting equation for the mass flow, which compensates for large pressure gradients, is shown in Eq. (4.17).

$$\begin{aligned} \frac{d\dot{m}_{i+1/2}}{dt}^{n+1/2} =& \frac{1}{\Delta x}[(\rho u^2 + p)_{i+1}^{m+1/2} - (\rho u^2 + p)_i^{m+1/2}]A_{i+1/2} + \\ &+ \frac{1}{\Delta x}\left[\varepsilon_{i+1}\frac{\dot{m}_{i+3/2}^m - \dot{m}_{i+1/2}^m}{\Delta x} - \varepsilon_i \frac{\dot{m}_{i+1/2}^m - \dot{m}_{i-1/2}^m}{\Delta x}\right] \end{aligned} \tag{4.17}$$

Control Volume - Method 3

The ROM model is presented in Stockar et al. (2013) and is as mentioned based on the same physical equations as 'Method 1 & 2' – the non linear Euler equations. The Euler equations are projected on Spatial Basis Functions (SBF) coupled to the partial differential equation states. The SBFs calculate the boundary values for the primary- and plug-control volumes. They are either coupled to the states with an empirical or polynomial approach, this means that a high precision

implementation could compensate for the intake manifold/primary pipes' geometry and measurements. A derivation of a general SBF can be found in Stockar et al. (2013).

$$\begin{aligned}
&\frac{\partial \rho A}{\partial t} + \frac{\partial \dot{m}}{\partial x} = 0 \\
&\frac{\partial \dot{m}}{\partial t} + \frac{\partial}{\partial x}\left(A\rho e_0(\gamma - 1) + \frac{\dot{m}^2}{\rho A}\right) = 0 \\
&\frac{\partial (\rho A e_0)}{\partial t} + \frac{\partial}{\partial x}\left[\dot{m} e_0 \gamma\right] = 0
\end{aligned} \tag{4.18}$$

$$\begin{aligned}
&\frac{\partial \rho A}{\partial t} + \frac{\partial \dot{m}}{\partial x} = 0 \\
&\frac{\partial \dot{m}}{\partial t} + \frac{\partial}{\partial x}\left(A\rho e_0(\gamma - 1) + \frac{\dot{m}^2}{2\rho A}(3 - \gamma)\right) = 0 \\
&\frac{\partial (\rho A e_0)}{\partial t} + \frac{\partial}{\partial x}\left[\gamma \dot{m} e_0 + (1 - \gamma)\left(\frac{\dot{m}^3}{2\rho^2 A^2}\right)\right] = 0
\end{aligned} \tag{4.19}$$

Table 4.1 shows the two simplest possible SBFs. Eq. (4.20) shows how the state values used in the SBF are computed, which is the mean value per length unit of either the control- or plug volumes.

Table 4.1: *Polynomial Spatial Base Functions. Can be extended to an arbitrary order of polynomials.*

Order	Formula
Constant	$\rho(t, x = L) = \rho_i^*$ $\dot{m}(t, x = 3L/2) = \dot{m}_{i-1/2}^*$ $e_0(t, x = L) = e_{0,i}^*$
Linear	$\rho(t, x = L) = \frac{\rho_i^* + \rho_{i+1}^*}{2}$ $\dot{m}(t, x = 3L/2) = \frac{\dot{m}_{i-1/2}^* + \dot{m}_{i+1/2}^*}{2}$ $e_0(t, x = L) = \frac{e_{0,i}^* + e_{0,i+1}^*}{2}$

$$\begin{aligned}
\rho^*(t) &= \frac{1}{L}\int_0^L \rho(t, x) dx \\
\dot{m}^*(t) &= \frac{1}{L}\int_{0.5L}^{1.5L} \dot{m}(t, x) dx \\
e_0^*(t) &= \frac{1}{L}\int_0^L e_0(t, x) dx
\end{aligned} \tag{4.20}$$

4.1.2 Courant-Friedricks-Lewy Criterion (CFL)

Courant et al. (1928) described a criterion which is necessary for convergence when solving partial differential equations, the critereon is shown in Eq.(4.21). This criterion makes sure that the distance traveled of the fluid information during computations is lower than the discretization length. This means that the information only travels to the connecting control volumes. Implicit solvers requires a lower C_{max} than explicit solvers, the C_{max} is typically set around 0.8.

$$C = \frac{u\Delta t}{\Delta x} \leq C_{max} \tag{4.21}$$

$$V = A \cdot L = A \cdot \Delta x \cdot n \Leftrightarrow \Delta x = \frac{V}{An} \tag{4.22}$$

$$C = \frac{uAn}{V}\Delta t \tag{4.23}$$

4.1.3 Adiabatic Intake Manifold

An adiabatic model of the entire intake manifold is a common way to obtain a zero-dimensional model. This model consists of one control volume which is similar to the staggered grid control volumes, as it is also derived from the mass- and internal energy balances. The governing state equations are shown in Eq. (4.24), and the pressure is calculated with the ideal gas law (see Eq. (4.5)).

$$\begin{cases} \frac{dm}{dt} = \dot{m}_{in} - \dot{m}_{out} \\ \frac{dT}{dt} = \frac{1}{mc_v}[\dot{m}_{in}c_v(T_{in} - T_{out}) + R(T_{in}\dot{m}_{in} - T_{out}\dot{m}_{out}) - \dot{Q}] \end{cases} \tag{4.24}$$

4.2 Heat Transfer

Heat transfer affects the intake manifold temperature when the fluid is flowing through the manifold and when the heated residual exhaust gases are mixed with the air from the intake manifold. Outside the cylinder most heat transfer comes from convection or conduction, while inside the cylinder radiation from the combustion also makes an addition, but can be neglected when then flame reaches the wall (Hamamoto et al., 1996).

4.2.1 Convection and Conduction

Convection is heat transfer from a flowing fluid to a solid. The rate of the heat transfer is decided by the fluid and the magnitude of the flow. Convection is described using Newton's law of cooling, where A is the effective area and h is in this case the heat transfer coefficient.

$$\dot{Q}_{conv} = hA\Delta T = hA(T - T_w) \tag{4.25}$$

The heat transfer coefficient is empirically described, in the following case as a function of flow speed (u) gathered from Eriksson and Nielsen (2014).

$$h = \begin{cases} 7.12u^{0.8} & \text{if } u \text{ is } \geq 5 \\ 5.8 + 4u & \text{if } u \text{ is } < 5 \end{cases} \tag{4.26}$$

Conduction is the transfer of heat within a solid where there is a temperature difference between its surface areas. Conduction is described with the following Equation if the solid is a square

$$\dot{Q}_{cond} = A\frac{k}{l}(T_1 - T_2) \tag{4.27}$$

and with the following equation if the heat is conducted through a pipe wall. Where A_i is the inner area (A=$2\pi r_i L$), r_i is the inner radius, r_0 is the outer radius and λ is the thermal conductivity of the material.

$$\dot{Q}_{conv} = A_i \frac{\lambda}{r_i ln\frac{r_0}{r_i}}(T_1 - T_2) \tag{4.28}$$

4.3 Cylinder and Combustion Modeling

A sufficient cylinder model will enable a simulation of the filling and emptying of the cylinder and manifold. Figure 4.3 shows how a usual cylinder pressure cycle looks like. The fresh air is added to the cylinder during the first expansion stroke, fuel is added either through the port simultaneously with the air or via a direct injection injector inside the cylinder. The air-fuel mixture is then compressed and usually somewhere during the compression stroke ignited. The combustion phase is entered when the air-fuel mixture has caught fire. The exact angle of when the combustion phase occurs is dependent on the ignition angle and thus allows it to occur either both during the compression phase or solely during the second expansion phase. The four stroke cycle is then completed with the second compression stroke where the exhaust gases is forced out of the cylinder.

The cylinder model needs to capture the varying cylinder volume, change of temperature, pressure, mass and the combustion. The heat transfer taking place is neglected in order to simplify the simulation. Heat transfer models can be added with the Woschni correlation (Woschni, 1967) – which compensates for convection and radiation heat transfer. The cylinder pressures will generally be higher than actual as a consequence of the disregarded heat losses.

4.3.1 In Cylinder Single-Zone Model

The single zone model works as a 'well stirred' single gas with uniform pressure, temperature and composition. The cylinder is either an open system or a closed system. It is considered an open system when the intake/exhaust valves are open and a closed system when the valves are closed. The general governing equations

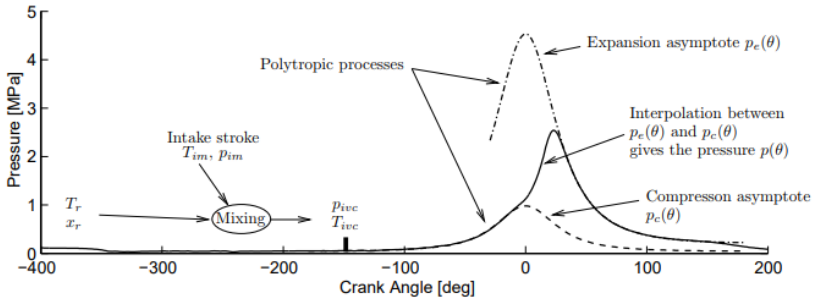

Figure 4.3: *Picture showcasing the procedure in the crank angle domain. The mixing process in the cylinder decides initial values for the combustion. Original figure from Eriksson and Andersson (2002).*

utilizes mass and energy balance and models the combustion as an heat addition. A first law of thermodynamics analysis for the cylinder volume gives the following equation

$$dU = dQ_{hr} - dW - dQ_{ht} + \sum_i H_i \tag{4.29}$$

where the last term is very broad and compensates for the energy flow in and out of the cylinder – both fuel and air. The equation can be constructed to depend on either time or crank angle. The volume expansion work is modeled with the basic expression for work $P = p \cdot v \Leftrightarrow dW = pdV$ and p is eliminated with the ideal gas law. Differentiation of the internal energy, insertion of the volume work and the ideal gas law gives Eq. (4.30). Which is the temperature governing equation (4.7) but with additional terms for heat transfer and heat release.

$$dT = -\frac{(\gamma - 1)RT}{V}dV + \frac{1}{mc_v}\left(dQ_{hr} - dQ_{ht} + \sum_i (h_i - u_i)dm_i\right) \tag{4.30}$$

The closed system model assumes that there is no mass transfer out of the cylinder, this assumption gives Eq. (4.31)

$$dT = -\frac{(\gamma - 1)RT}{V}dV + \frac{1}{mc_v}\left(dQ_{hr} - dQ_{ht}\right) \tag{4.31}$$

The pressure change is calculated with the ideal gas law and effects due to cylinder leakage and crevice volumes are neglected.

4.3.2 Net Heat Release

The heat release can either be calculated in a backwards or forwards manner. A backwards manner means that the heat release is calculated using measured cylinder pressures. A forwards manner uses the heat release as an input, and gives the cylinder pressure as an output. The measured pressure gradient can

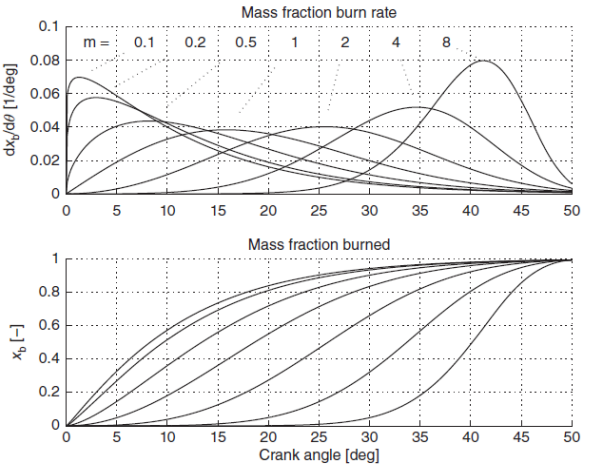

Figure 4.4: *Tuning parameters a and θ_{comb} is set to 5 and 50 °. Original figure is presented by Eriksson and Nielsen (2014).*

be derived for whichever scalar that is desired, a common scalar is the cylinder crank angle. The volume (V) in the cylinder is dependent on the crank angle and thus that relation also need to be defined. These types of analysis is further explained in Eriksson and Nielsen (2014). In this case the net heat release is modeled by approximating the combustion with the well known Vibe function (Vibe and Meißner, 1970). The Vibe function is applied when approximating the mass fraction burned, MFB (x_b), shown below

$$x_b = 1 - e^{-a\left(\frac{\theta-\theta_{SOC}}{\Delta\theta_{comb}}\right)^{m+1}} \tag{4.32}$$

and on its differentiated form describing the burn rate

$$\frac{dx_b(\theta)}{d\theta} = \frac{a(m+1)}{\Delta\theta_{comb}}\left(\frac{(\theta-\theta_{ig})}{\Delta\theta_{comb}}\right)^{m} e^{-a\left(\frac{\theta-\theta_{SOC}}{\Delta\theta_{comb}}\right)^{m+1}} \tag{4.33}$$

θ represents the crank angle, θ_{SOC} is the angle where the combustion starts, θ_{comb} is the combustion duration and a and m are tuning parameters. Figure 4.4 shows how the mass fraction functions depends on the m tuning parameter. The tuning parameters a and m is coupled to the physical domain via a dependency of flame development angle (θ_d) taking place between ignition and 10 % MFB, and a fast burn angle (θ_b) taking place between 10-85 % MFB (Heywood, 1988). Thornberg and Eriksson Kraft (2018) presents how the tuning parameters are optimized to fit a measured pressure trace. As the Vibe function is over parameterizated one of the parameters has to be fixed in order to get a unique

solution. If the combustion duration $\Delta\theta_{comb}$ is fixed the parameters become

$$m = \frac{ln\left(\frac{ln(1-0.1)}{ln(1-0.85)}\right)}{ln(\Delta\theta_d) - ln(\Delta\theta_d + \Delta\theta_b)} - 1 \tag{4.34}$$

$$a = -ln(1-0.1)\left(\frac{\theta}{\Delta\theta_d}\right)^{m+1} \tag{4.35}$$

$$\Delta\theta_{comb} \approx 2\theta_d + \theta_b \tag{4.36}$$

The heat release added to (4.31) is calculated with

$$\frac{dQ_{hr}}{d\theta} = Q_{in}\frac{dx_b}{d\theta} \tag{4.37}$$

where Q_{in} represents the energy added by the fuel and is described with the following equation

$$Q_{in} = m_f q_{HV} \eta_f \tag{4.38}$$

where q_{HV} is the specific *lower* heating value of the fuel, which compensates for the energy loss caused by evaporated fuel, m_f is the fuel mass and η_f is the combustion efficiency. If the model is dependent on integrating with respect to time, such as a Simulink model, a scaling factor converting to a time dependence is needed i.e. using the substitution of $dt = d\theta/\omega$. The amount of fuel could be modeled with great accuracy if the fuel injector module was modeled, but a simpler approach would be to assume instant injection modeled with the following equation

$$\dot{m}_f = \frac{\dot{m}_{ac}}{\lambda\left(\frac{A}{F}\right)_s} \cdot (1 - x_r) \tag{4.39}$$

and integrated over the air charge duration i.e. between IVO and IVC to achieve the total mass of fuel added.

4.3.3 Thermodynamic Parameter Model

In order to sufficiently and accurately model the pressure and temperature changes in the cylinder during the large span of temperatures occurring between IVO and EVC, changes in the thermodynamic parameters is needed. Klein (2007) concluded that γ is the most imminent variable when calculating the heat release rate. The model used in this thesis was presented by Gatowski et al. (1984) which is a linear model and thus quite simple, the model is presented in Eq. (4.40). Klein (2007) also presented a more advanced model with higher accuracy.

$$\gamma(T) = \gamma_{300} + b(T - 300) \tag{4.40}$$

Model parameters can be approximated as $\gamma_{300} \approx 1.35$ which is the heat capacity ratio of air at 300 K and $b \approx 7 \cdot 10^{-5}$.

4.3.4 Residual Gas

The residual gas is trapped exhaust gas in the cylinder from previous combustions. There are many methods to estimate this parameter, some methods are described in Nikkar (2017). The residual gas in the simulation models are approximated as the remaining mass in the cylinder at EVC. The residual gas is calculated with the following equation

$$x_r = \frac{m_{cyl,EVC}}{m_{cyl,EVC} + m_{air,IVC}} \tag{4.41}$$

where no bookkeeping is done in order to compensate for possible residual gas staying in the cylinder during multiple cycles. This equation is only valid when there is negative overlap.

4.3.5 Cylinder Geometry

The following equation describes the cylinder volume, which is needed in the open and closed cylinder models.

$$V(\theta) = V_d\left(\frac{1}{r_c - 1} + \frac{1}{2}\left(\frac{l}{a} + 1 - \cos\theta - \sqrt{\left(\frac{l}{a}\right)^2 - \sin^2\theta}\right)\right) \tag{4.42}$$

$$V_d = \frac{\pi B^2 L}{4} \tag{4.43}$$

Where V_d is the maximum displacement volume, r_c is the compression ratio, l is the connecting rod length and a is the crank radius. Figure 4.5 puts the geometric parameters into context.

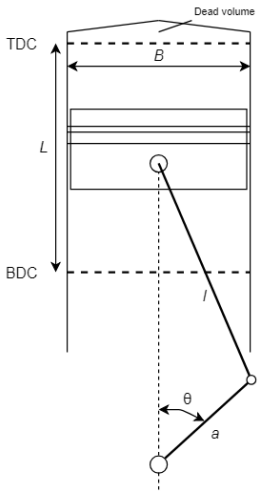

Figure 4.5: *Geometry of the cylinder.*

4.4 Compressible Flow Model

The mass flows through the throttle, intake and exhaust valves during sonic and sub-sonic velocities. When the flow happens at such high velocities a compressible model is needed to accurately describe the flow. The base equation of a flow through a restriction is based on the following assumptions: the fluid is compressible, mass is not moving before the restriction, no heat transfer and that the process is reversible. Heywood (1988) has derived the model in his Appendix C and the result is as follows

$$\dot{m} = C_d A \frac{p_{up}}{\sqrt{RT_{up}}} \Psi(\Pi) \tag{4.44}$$

where

$$\Pi = \frac{p_{down}}{p_{up}} \tag{4.45}$$

$$\Psi = \begin{cases} \sqrt{\gamma \left(\frac{2}{\gamma+1}\right)^{\left(\frac{\gamma+1}{\gamma-1}\right)}} & \text{if } \Pi < \frac{2}{\gamma+1}^{\frac{\gamma}{\gamma-1}} \\ \Psi_0 & \text{if } \frac{2}{\gamma+1}^{\frac{\gamma}{\gamma-1}} > \Pi > \Pi_{lin} \\ \Psi_0(\Pi_{lin}) \frac{1-\Pi}{1-\Pi_{lin}} & \text{otherwise} \end{cases} \tag{4.46}$$

$$\Psi_0 = \sqrt{\frac{2\gamma}{\gamma-1}\left(\Pi^{\frac{2}{\gamma}} - \Pi^{\frac{\gamma+1}{\gamma}}\right)} \tag{4.47}$$

A linearized part of the Ψ-curve is used in order to decrease the computational cost, a lower Π_{lin} results in faster but less accurate simulations. Figure 4.6 shows how the Ψ functions varies with the pressure ratio (Π). The area marked around pressure ratio 0.9 shows the interval where a linearization is of interest in terms of computational cost. It is of interest since a small change in pressure ratio results in big change in terms of Ψ value, therefore small computational fluctuations in terms of Π would cause oscillations. As the mass flows from a higher pressure to the lower pressure this model can be used for flows in both directions. Which is a common scenario for the intake valve, where the mass usually flows out of the cylinder during the beginning and ending of the valve flow process (Heywood, 1988).

4.5 Valve Mechanics

The intake and exhaust valves are controlled with two cam axles which mechanically pushes the valves between an open and closed state. The cam axles are synced with the engine rotational speed with a timing belt connected to the crank axle.

The four stroke engine cycle contains of, as discussed in Section 2.2, two compression- and expansion strokes - during a total of two revolutions. The intake valve is usually opened somewhere between the end of the second compression stroke and the first expansion stroke. The exhaust valve is usually opened

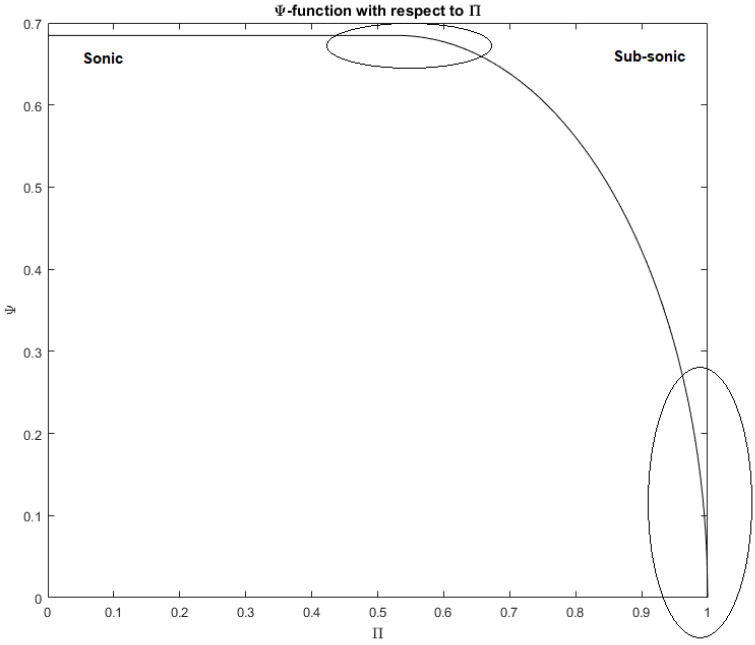

Figure 4.6: *Ψ function with highlighted problematic Π-values, simulated with $\gamma = 1.4$. Π_{crit} is the point where the flow shifts between sonic and sub-sonic. The second marked area is where a linearization of Ψ is reasonable.*

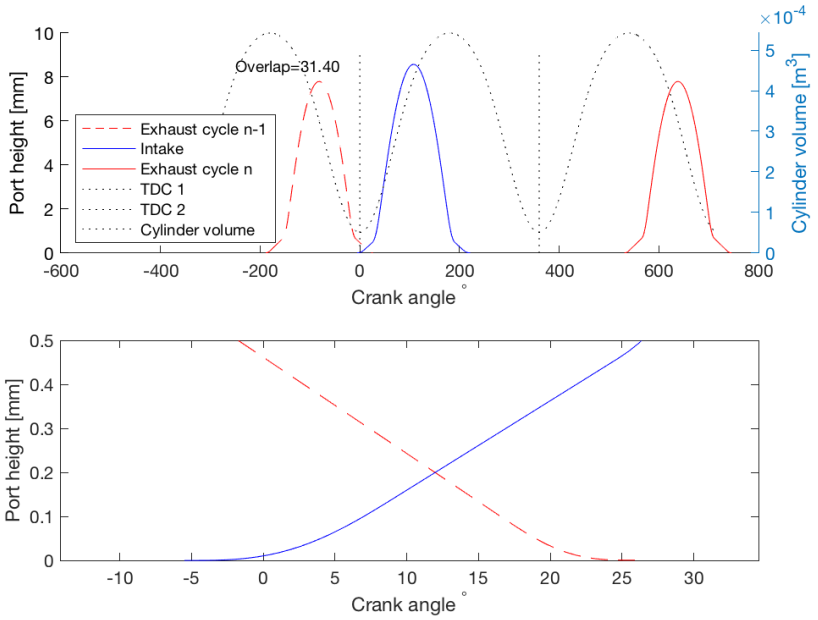

Figure 4.7: *Figure showing the lifts of the intake and exhaust valves. The overlap in this the particular case is 31.4° and is displayed in the bottom picture.*

somewhere towards the end of the second expansion stroke and closed between the end of the second compression stroke and the first expansion stroke. The exact angle where the valves open and close is usually variable with an opportunity to phase shift the cam axles. Figure 4.7 shows how the valve lifts as a function of crank angle. In this case the overlap is 31.4 °, but can be phased into a negative overlap. The crank angle timing are defined from their positions furthest away from each other, i.e a phase shift of 10 degrees puts either valve timing 10 degrees close to the others default position. The shape of the cams can be approximated with the following geometric functions expressed for the case of an intake valve or exhaust valve.

$$\text{pos} = \begin{cases} 1 - \cos^2\left(\frac{\theta - \theta_{IVO,corr}}{(\theta_{IVC}+\theta_{IVO,corr})/2} \cdot \frac{\pi}{2}\right) & \theta \geq \theta_{IVO}, \theta < (\theta_{IVO,corr} + (\theta_{IVC} + \theta_{IVO,corr})/2) \\ \cos^2\left(\frac{\theta - (\theta_{IVC} - (\theta_{IVC} - \theta_{IVO,corr})/2)}{(\theta_{IVC}+\theta_{IVO,corr})/2} \cdot \frac{\pi}{2}\right) & \theta \geq (\theta_{IVC} - (\theta_{IVC} - \theta_{IVO,corr})/2), \theta \leq \theta_{IVC} \\ 0 & \text{otherwise} \end{cases} \tag{4.48}$$

Table 4.2: *Geometric valve parameters.*

Lift height	L_v
Head diameter	D_v
Seat width	w
Seat angle	β
Stem diameter	D_s
Mean seat diameter	$D_m (= D_v - w)$
Port diameter	D_p

$$\text{pos} = \begin{cases} 1 - \cos^2\left(\frac{\theta - \theta_{EVO}}{(\theta_{EVC,corr} - \theta_{EVO})/2} \cdot \frac{\pi}{2}\right) & \theta \geq \theta_{EVO}, \theta < (\theta_{EVO} + (\theta_{EVC,corr} - \theta_{EVO})/2) \\ \cos^2\left(\frac{\theta - (\theta_{EVC,corr} - (\theta_{EVC,corr} - \theta_{EVO})/2)}{(\theta_{EVC,corr} - \theta_{EVO})/2} \cdot \frac{\pi}{2}\right) & \theta \geq 4\pi - (\theta_{EVC,corr} - \theta_{EVO})/2, \theta \leq 4\pi \\ k\theta + m & \theta \geq, \theta \leq \theta EVC \end{cases} \tag{4.49}$$

Where $\theta_{IVO,corr}$ is the corrected value if it is phase shifted past TDC. A phase shift past TDC also means that you need to correct the first if statement. Similar compensation for θ_{EVC} is needed. Parameters k and m are linearization parameters from TDC to EVC.

The opening area is modeled as a function of the valve lift height and geometry of a poppet valve described in Heywood (1988).

$$\text{A} = \begin{cases} \pi L_v \cos(\beta)(D_v - 2w + \frac{L_v}{2}\sin(2\beta)) & \text{if } L_v > 0, L_v < \frac{w}{\sin(\beta)\cos(\beta)} \\ \pi D_m \sqrt{(L_v - w\tan(\beta))^2 + w^2} & \text{if } L_v > \frac{w}{\sin(\beta)\cos(\beta)}, L_v < w\tan(\beta) + \sqrt{(\frac{(D_p^2 - D_s^2)}{4D_m}) - w^2} \\ \frac{\pi}{4}(D_p^2 - D_s^2) & \text{if } L_v > w\tan(\beta) + \sqrt{(\frac{(D_p^2 - D_s^2)}{4D_m}) - w^2} \\ 0 & \text{otherwise} \end{cases} \tag{4.50}$$

An explanation of the valve geometry parameters is shown in Table 4.2 and the lift height is in this case approximated as *pos* multiplied with the maximum lift height. Higher precision simulations would use mapped data. The discharge coefficients are implemented to emulate the plots presented by Heywood (1988), the implemented discharge coefficients are shown in Figure 4.8.

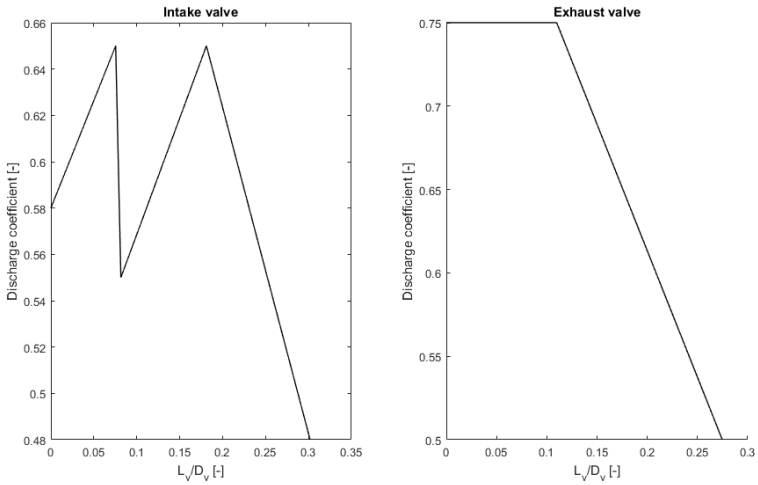

Figure 4.8: *Figure showing the intake and exhaust discharge coefficients as a function of valve lift and valve head diameter.*

5

Test Setup

The goal of the testing is to gather validation data to compare with simulated data, with the main focus on temperature measured with extraordinary fast temperature sensors. A comprehensive overview and reasoning of the test plan can be found in Section 5.4. The testing was done at the vehicular systems department at Linköping University with a test engine supplied by VCC, which was a turbocharged gasoline engine. Corresponding commercial engine name would be a T3, T4 or T5. The engine is, on command, software controlled with a program called INCA, sold by ETAS. Table 5.1 shows the engine and volume specification. Figure 5.1 shows a picture of the test engine with the temperature sensor module mounted on the intake manifold.

Table 5.1: *Engine specification.*

Cylinder volume	2.0 l
Cylinders	Inline 4
Compression ratio	10.8
Bore	82 mm
Stroke	93.2 mm
Exhaust manifold	2 l
Intake manifold (plastic)	2 l
Pipe volume (approx.)	0.157 l
Effective intake volume	$2\,\text{l} + 8 \cdot 0.157\,\text{l}$

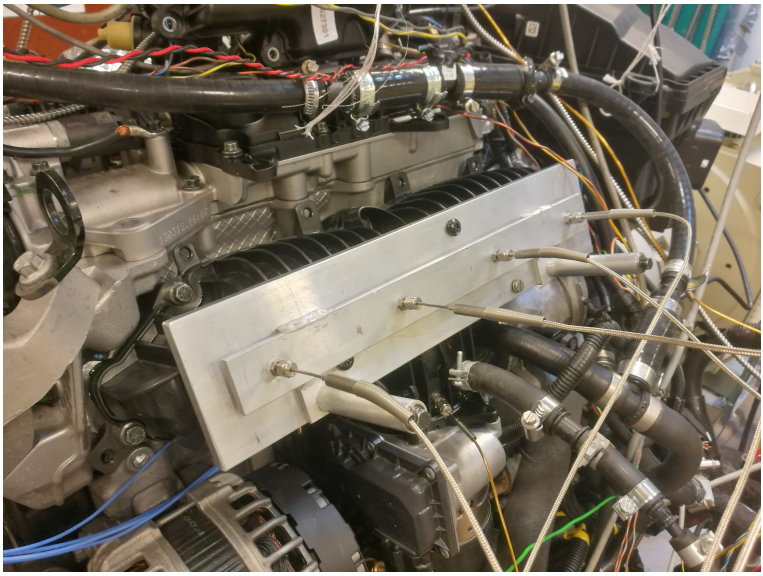

Figure 5.1: *Volvo test engine with the temperature module mounted on the intake manifold.*

5.1 Data Sampling

As mentioned above, the main focus is to capture the fast temperature transients accurately. But to analyze the effects of the built in ECU-control most ECU data is sampled as well. Furthermore, the cylinder pressure is also sampled which can be used to approximate the combustion Vibe-parameters and compared to simulation values.

The intake temperatures and pressures are sampled at 1000 Hz, this sampling rate is feasible as it captures 1000 samples during the transient which usually occurs during one second, see Section 6. The temperature sensor, a MEDTHERM fine wire probe, with a time constant of 4-5 ms. The sensor dynamics are captured in simulations with a first order filter with the sensor time constant and sampling frequency. The pressure is measured with previously mounted sensors, the exact placement of the pressure sensor is considered indifferent since the pressure can be assumed to propagate at the speed of sound.

5.2 Temperature Sensor Placement

The sensor placement is sensitive with respect of the air getting hotter closer to the valves, both due to successively hotter air getting compressed and eventual influence from backflow of residual gas. Furthermore, the cylinders are not working in conjunction in a manner that is not known to the sampled signals from the ECU, this means that the timing with respect to the mass flow at the sensor varies

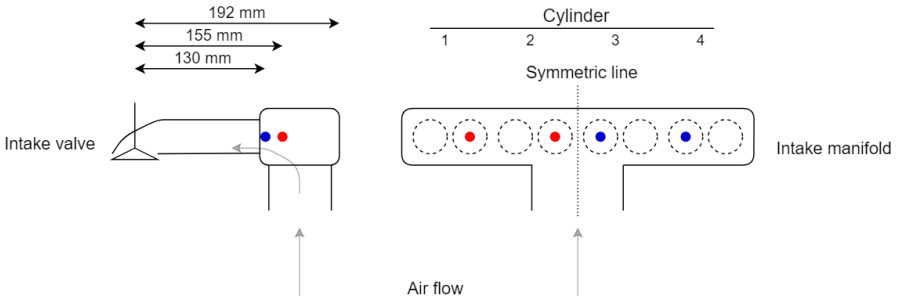

Figure 5.2: *Figure showing the sensor setup. The red and blue dots represents the mounted temperature sensors. The left picture represents the pipes running down to the cylinders. Each cylinder has two separate intake valves and pipes.*

unpredictably from test to test. This means that the maximum transient temperature could vary from test to test. Two temperature sensors were placed as close to the valves as possible and two at a slightly longer distance to the valves, this was done in order to get two validation points. The positioning of the sensor is important since it is a wire probe, the wire should be placed perpendicular to the mass flow in order to maximize the exposure to the mass flow. Both sensors were slightly at angle to mitigate this. Figure 5.2 shows how the sensors were placed.

5.3 Pegging the Cylinder Pressure

Pegging is the name of the process when you sync the sensor data, often sampled in Volt, and convert it into a chosen pressure scale. There are many methods to complete this process, simpler processes which impose certain model inaccuracies and more complex methods which considerably reduce these uncertainties. Kangyoon et al. (2008) presents a study on different pegging methods. Methods syncing the pressures at intake-BDC, using several reference points or a least squares method is presented. Syncing the pressures at intake-BDC is the simplest and induces measurement noise uncertainties, but this is for simplicity reasons the method that is used in this thesis (Kangyoon et al., 2008).

5.4 Tests

Since the transient behaviour is of interest all tests are dynamic and defined either by a step up and down in throttle position or intake manifold pressure. Every up and down step is given around 40 seconds in order to ensure stationarity between the steps. A total of 101 different tests have been done, varying different engine parameters in order to detect trends and isolate certain effects coupled to different control signals. The VVT, turbo and throttle time constant has in different variations been tested for engine speeds between 800 RPM- 2500 RPM. A full

test list can be found in Appendix A.

- Locked VVT, negative overlap - 8.6 degrees between EVC and IVO.
  - This is done with the purpose of minimizing backflow effects.
- Free VVT, intake and exhaust camshaft controlled by ECU.
  - This is done to see the influence of the current VVT-control.
- Varying VVT-settings
  - Intake- and exhaust-VVT varied independently in order to isolate their separate effects.
- Varying throttle ramping time
  - This is done to see the influence of a changed pressure step time constant.
- Turbo-boosted pressure transient
  - Made to see the effect of the slower turbo pressure gradient. This is tested solely with free VVT.

6
Results

The modeling, simulation and testing processes resulted in three types of results, the first being related to the simulation setup, the second being related to validating the intake fluid dynamics compared to measurements and the last being a sensitivity analysis. All tests were made with a locked VVT setting which gave a gap of about 8.6° between EVC and IVO, if not stated otherwise.

6.1 Simulation Setup

First of all is the different intake manifold models compared to each other, this is followed up with an analysis of the importance of the amount of Control Volumes that are simulated.

6.1.1 Control Volume Setup

The intake is modeled as a straight pipe. An effective area is calculated in order to maintain the volume and length constant. As the curvatures in the pipe and filling volume are approximated as straight the pressure gradients should become a little to steep, as Renberg (2008) concluded. Some version of volumetric efficiency is included as discharge coefficients are approximated and included in the simulation model. Figure 6.1 shows how the intake and exhaust manifolds are modeled, where the intake, in this case, is modeled with ten control volumes and the exhaust with one control volume.

A matching control volume for any given point in the manifold is calculated with the following equation

$$CV = ceil\left(\frac{L_{tot} - L_{point}}{L_{CV}}\right) \tag{6.1}$$

where L_{tot} is the total volume length, L_{point} is the distance from the point to the ending of the volume and L_{CV} is the length per each control volume. The corresponding control volume is the CV-value rounded towards positive infinity (MATLAB-function *ceil*). The length used in the simulation is approximated as the length from the intake manifold wall to the stem pipe of the intake valve, this length is shown in Figure 5.2. The temperature sensors' position in a 10 control volume configuration is shown in Figure 6.1. The effective cross sectional area of the 1-D interpretation is calculated as the total volume divided by the approximated length of the intake system.

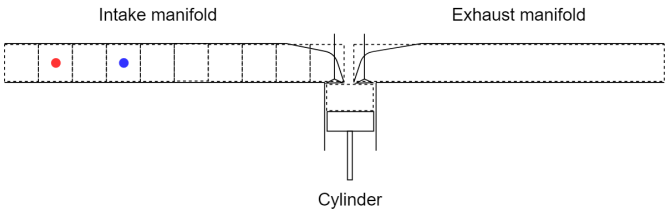

Figure 6.1: *Picture showing the control volume setup. The intake manifold is 1-D modeled with 10 control volumes, the cylinder and exhaust manifold are 0-D modeled. The blue and red dots represents the temperature sensor positions*

6.1.2 Simulation comparison between '*Method 1*', '*Method 2*' & '*Method 3*'

Method 1, *Method 2* and *Method 3*, described in Section 4.1.1, is tested, under comparable conditions i.e. with the same initial states, thermodynamic parameters and geometry, with a step up and down in mass flow. That means that the pressure in the intake manifold is built up as it is filled with more air. The mass flow into the engine is simulated with a Mean Value Engine Model and the mass flow into the manifold is given as a fixed input in order to ensure that it is the intake manifold dynamics contributing to the computational requirements. All models are simulated with two control volumes since it will simplify the comparison among them. Figure 6.2 shows how the pressure, temperature and mass flows varies during the test sequence. *Method 1* and *Method 2* shows *very* similar temperatures as they are stacked on each other in the figure. This is reasonable since they are using the same control volume governing equations. The two different plug volume models also seem to result in very similar results as the pressure propagations also are very similar. *Method 3* deviates from *Method 1* and *2* as the pressures propagates slower, the propagation is also clearly dependent on the chosen SBF function. The linear SBF, which basically is a moving average filter between two control volumes/plugs logically decreases the pressure gradient. Furthermore *Method 3* shows a different temperature transient, with lower maximum temperatures and shorter transient duration. Table 6.1 shows the minimum required time step for each method. The minimum required time step was

Table 6.1: *Minimum required time step for each method.*

Method 1 (Öberg)	3300 Hz
Method 2 (3DCell)	17500 Hz
Method 3.1 (ROM con)	3200 Hz
Method 3.2 (ROM lin)	2800 Hz

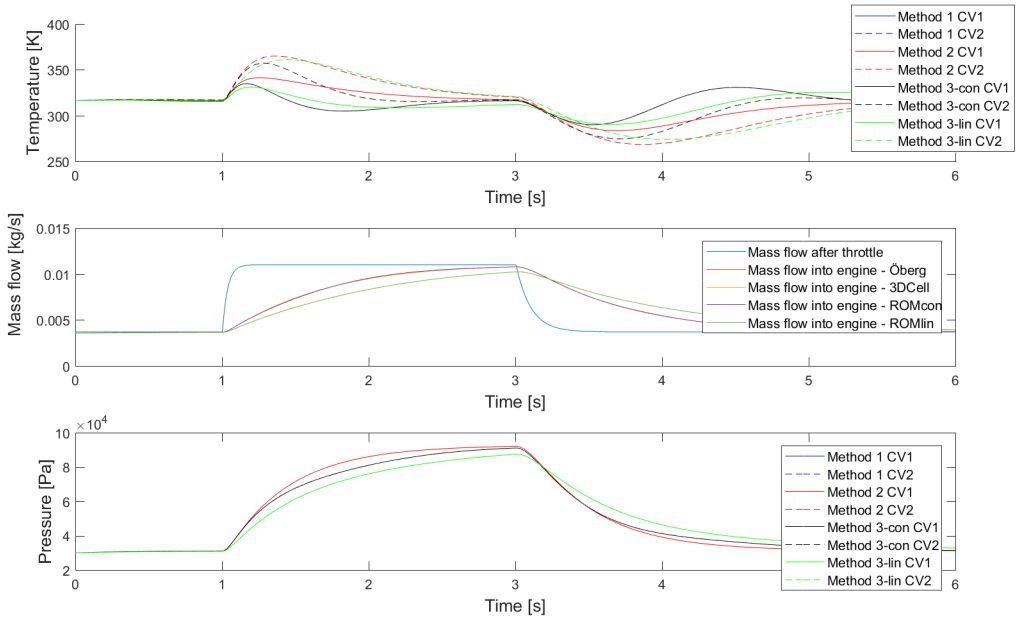

Figure 6.2: *Comparison of each intake dynamics model. Method 1 & 2 are very close to each other or completely matching each other.*

evaluated for this specific tested pressure step and could be approximated with the CFL-criterion presented in Courant et al. (1928), but the presented numbers are approximated via trial and error with an *ode3* solver.

6.1.3 Temperature and Time-step Correlation

The choice of the amount of control volumes is not obvious, Figure 6.3 shows a run down of max temperatures and time step sizes as the amount of control volumes varies for *Method 1*. The changed maximum temperature is interpreted as a leading indicator of how much information that is lost due to a sparse control volume setup. The maximum temperature increases with the amount of control volumes. The temperature rise between each level decreases as you go higher, between 6 and 10 CVs there is a 1.256 % heightening in temperature but a signif-

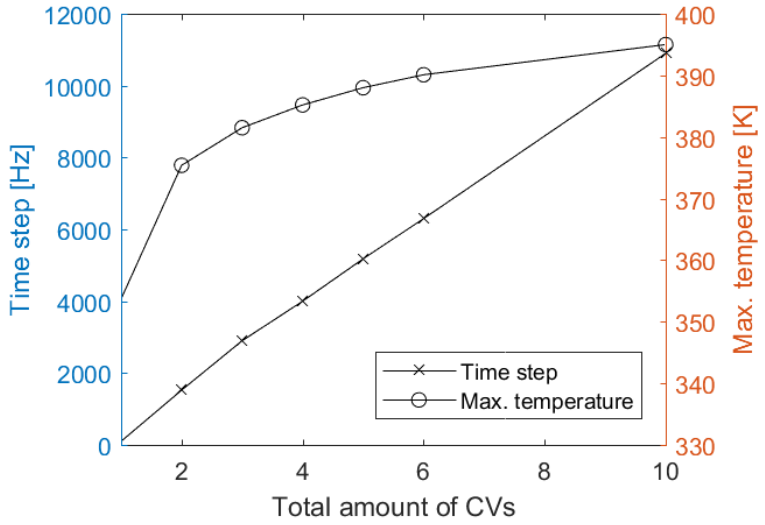

Figure 6.3: *Time step and maximum temperature correlation with the amount of control volumes.*

icantly higher rise in its time step demand. Therefore going beyond 10 control volumes would render in a slightly increased maximum temperature but at a significant computational cost, which is in line with the CFL-criterion presented in Section 4.1.2. Table 6.2 puts the time step requirements into a time perspective. But the main objective of increasing the amount of control volumes is to increase the temperature accuracy at a certain point in the manifold, this being right at the intake port or at a measurement point.

Table 6.2: *Computational time for each amount of control volumes.*

Amount of CVs	Computational time [s]
1	0.15
2	0.20
3	0.3
4	0.39
5	0.4628
6	0.56
10	0.98

6.2 Full Model Simulation

This section will compare a measured temperature with its corresponding control volume in a *Method 1* one-dimensional intake manifold with 10 control volumes.

Table 6.3: *Accuracy for 800 RPM 32kPa-81kPa during the positive and negative transient.*

	RMSE- up	Max dev - up	RMSE- down	Max dev - down
Method 1	2.47	1.32 %	7.57	5.55 %
Adiabatic CV	17.77	10.82 %	20.25	10.5 %

A comparison with the the adiabatic control volume model is also included. If not mentioned – assume the 155 mm sensor position in cylinder one. The transients will be validated for three different engine RPM and two different pressure steps for each engine RPM.

6.2.1 Temperature Transient Validation

This section compares the positive and negative temperature transients. The pressure dynamics has been calibrated to match the measurements as good as possible. No heat transfer is simulated in neither case. As a consequence of this the inlet temperature of the simulations are matched with the stationary temperature of the measurements precisely before the pressure step. Figure 6.4 and 6.5 shows the validation plots for the positive and negative temperature transient at 800 rpm. Table 6.3 and 6.4 shows corresponding model performance indicators, these values reflects the figures very well; as the positive transients generally matches the measurements better than the negative transients. A faster positive transient for *Method 1* has a good agreement at all temperatures, and deviates less than 1 % from the maximum measured temperature. But its faster transients hurts its RMSE-value. The time duration of its positive transients corresponds well with the measured temperature. The effect of having no heat transfer can be seen in the stationary temperature after the transient in Figure 6.4b, since the measurements temperature slowly deviates from *Method 1*. The adiabatic 0-D model lacks information in order to predict the specific measurement position and is very influenced of backflow. The backflow increases the stationary temperature when the intake pressure is low, and the stationary temperature is decreased when the intake pressure is increased since the backflow decreases with an increased intake manifold pressure. The adiabatic model is struck extra hard of the backflow since it assumes instant dissipation in its entire control volume. The modeled negative transients shows a generally bad agreement with the measurement. This is reflected in the models' performance indicators. The measured negative transients for the slower pressure transients, see e.g. Figure 6.5a, shows a transient that solely decreases its temperature. However, the measured negative transients for the faster pressure transient, see e.g. Figure 6.5b, shows a transient temperature that both increases and decreases. The temperature also influences the intake pressure.

Figure 6.6 and 6.7 and Figure 6.8 and 6.9 shows the validation plots for the positive or negative temperature transients for 1000 RPM and 1500 RPM. Their corresponding performance indicators are shown in Table 6.5, 6.6 and Table 6.7, 6.8. The general trends are intact through the different engine speeds. With

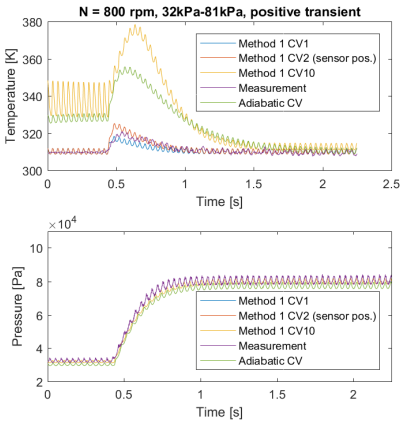

(a) A slow temperature and pressure transient at 800 RPM. Positive pressure gradient.

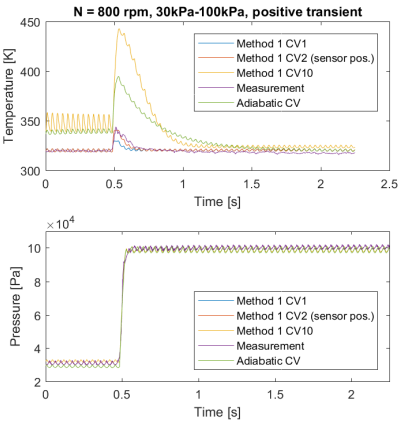

(b) A fast temperature and pressure transient at 800 RPM. Positive pressure gradient.

Figure 6.4: *Positive pressure gradient transients at 800 RPM.*

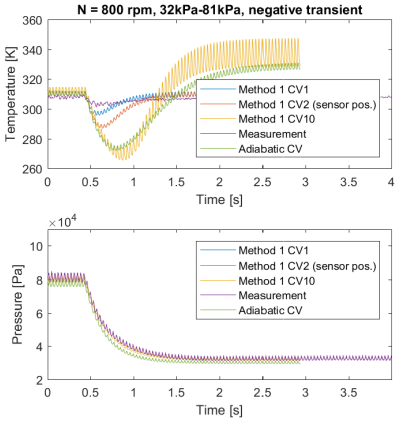

(a) A slow temperature and pressure transient at 800 RPM. Negative pressure gradient.

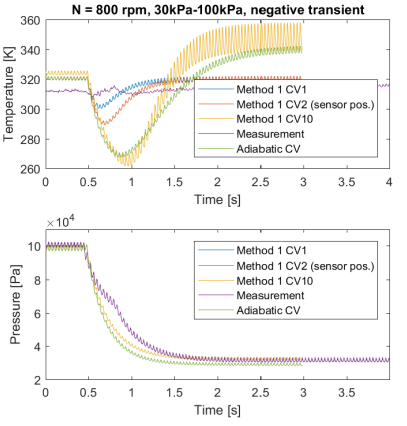

(b) A fast temperature and pressure transient at 800 RPM. Negative pressure gradient.

Figure 6.5: *Negative pressure gradient transients at 800 RPM.*

Table 6.4: *Accuracy for 800 RPM 30kPa-100kPa during the positive and negative transient.*

	RMSE- up	Max dev - up	RMSE- down	Max dev - down
Method 1	2.96	-0.995 %	10.93	7.78 %
Adiabatic CV	20.8	14.75 %	229.5	14.7 %

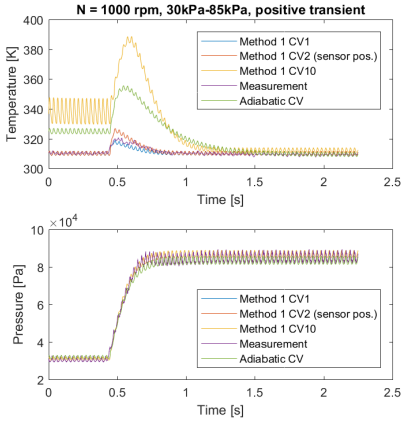

(a) A slow temperature and pressure transient at 1000 RPM. Positive pressure gradient.

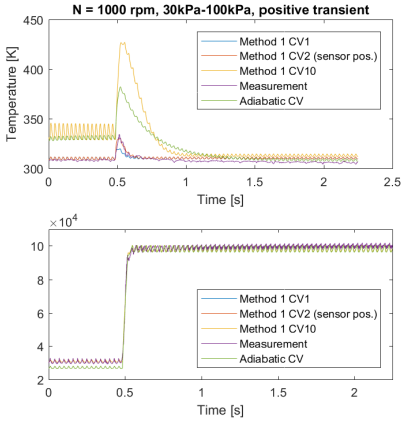

(b) A fast temperature and pressure transient at 1000 RPM. Positive pressure gradient.

Figure 6.6: *Positive pressure gradient transients at 1000 RPM.*

Table 6.5: *Accuracy for 1000 RPM 30kPa-85kPa during the positive and negative transient.*

	RMSE- up	Max dev - up	RMSE- down	Max dev - down
Method 1	2.6	1.93 %	7.42	5.92 %
Adiabatic CV	15.59	11.43 %	19.4	11.3 %

better accuracy during positive transients and bad accuracy during negative transients.

6.2.2 Temperature Transient Correlation with in-cylinder Temperature

The adiabatic model and *Model 1* are run for a slow and fast temperature transient at 800 RPM. Figure 6.10 shows all modeled intake manifold temperatures as well as their corresponding simulated in-cylinder temperatures at IVC, i.e. one temperature for each simulated cylinder cycle and may therefore seem a bit choppy in the figure. Figure 6.11 shows the simulated cylinder pressures for *Method 1*, the

Table 6.6: *Accuracy for 1000 RPM 30kPa-100kPa during the positive and negative transient.*

	RMSE- up	Max dev - up	RMSE- down	Max dev - down
Method 1	2.19	-1.16 %	10.05	7.29 %
Adiabatic CV	18.99	14.28 %	27.98	15.75 %

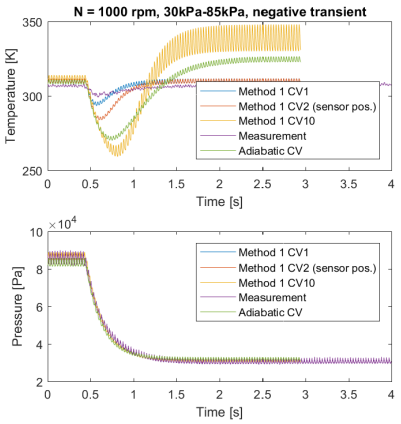

(a) A slow temperature and pressure transient at 1000 RPM. Negative pressure gradient.

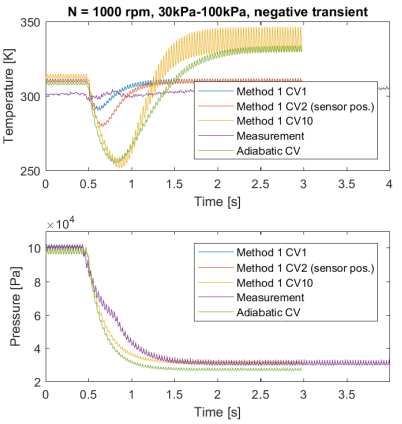

(b) A fast temperature and pressure transient at 1000 RPM. Negative pressure gradient.

Figure 6.7: *Negative pressure gradient transients at 1000 RPM.*

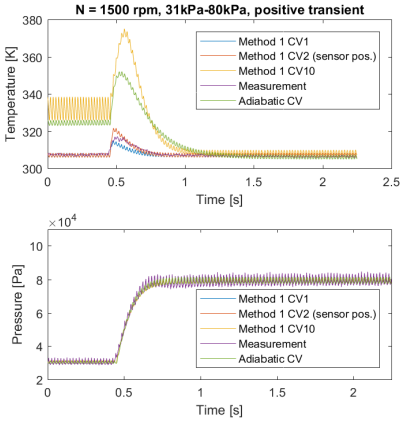

(a) A slow temperature and pressure transient at 1500 RPM. Positive pressure gradient.

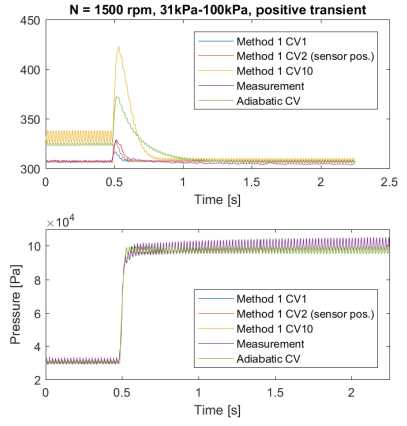

(b) A fast temperature and pressure transient at 1500 RPM. Positive pressure gradient.

Figure 6.8: *Positive pressure gradient transients at 1500 RPM.*

Table 6.7: *Accuracy for 1500 RPM 31kPa-80kPa during the positive and negative transient.*

	RMSE- up	Max dev - up	RMSE- down	Max dev - down
Method 1	1.94	1.43 %	6.69	4.86 %
Adiabatic CV	13	11.01 %	20.27	10.53 %

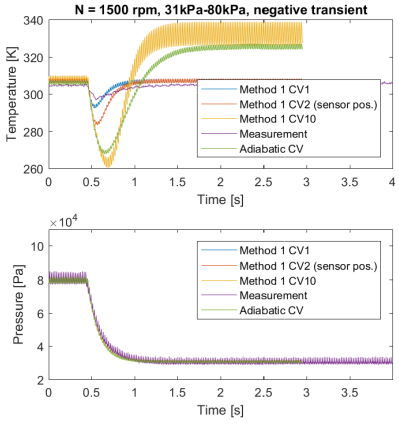

(a) A slow temperature and pressure transient at 1500 RPM. Negative pressure gradient.

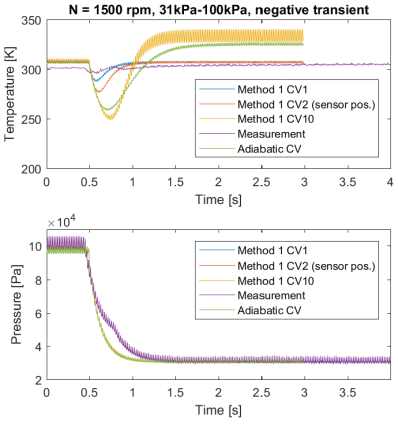

(b) A fast temperature and pressure transient at 1500 RPM. Negative pressure gradient.

Figure 6.9: *Negative pressure gradient transients at 1500 RPM.*

Table 6.8: *Accuracy for 1500 RPM 31kPa-100kPa during the positive and negative transient.*

	RMSE- up	Max dev - up	RMSE- down	Max dev - down
Method 1	3.53	-0.456 %	10	7.38 %
Adiabatic CV	14.07	13.3 %	26.05	14.3 %

adiabatic model as well as a measured cylinder pressure during a corresponding test session. The measured cylinder pressure is pegged as described in Section 5.3 – only pegged for one cycle and assumed to be true for all cycles. The consequence of this can be seen in it's plot since the intake pressure level varies when it should be somewhat constant. The constants used to simulate the combustions are the same for both *Method 1* and the adiabatic model. These parameters were chosen to a neutral pressure curve - with no delayed ignition tendencies or other effects ($\theta_d = 8.58°$, $\theta_b = 8.14°$, $\theta_{SOC} = 325°$ i.e. an early combustion), but no direct physical link to the actual test was used.

6.3 Test Data Results

This section focuses on presenting test cell results with varying engine settings and highlighting the effects that these settings has on the transient temperature.

6.3.1 Pressure Gradient & Engine Speed

The plots in Section 6.2 hints to a dependence on the pressure difference change in the intake manifold. Figure 6.12 shows how the absolute temperature differences and pressure differences for each test made in Section 6.2. The points at a pressure differences below 60kPa are the tests named ”slow transient” and the points above represents the ”fast transients”. A positive pressure gradient has a clear trend; a lower pressure difference results in a lower temperature difference and a higher pressure difference results in a higher temperature difference, which is true for simulations and measurements. The negative pressure gradient proves still to be difficult to analyze. Figure 6.13 shows how the time constant impacts the transient temperatures, the increased throttle ramping time increases the intake pressure time constants which clearly impacts the temperature transient behaviour. The intake pressure is increased during additional cycles and therefore the transient temperature is decreased by a closer balance between the in- and out mass flow. An increased engine speed should theoretically increase the positive pressure change time constant and decrease the negative pressure change time constant. However, the effect of that is hard to decipher in Figure 6.12. Figure 6.14 shows equivalent pressure steps for four different engine speeds: 800, 1000, 1500 and 2500 rpm. The positive temperature transient, seen in Figure 6.12a, clearly trends towards a lower maximum for a higher engine speed. The length of the transient is also shortened with a higher engine speed. The negative temperature transient, seen in Figure 6.12b, has a clear trend where the temperature reduction gets bigger for a higher engine speed. This is due to the increasingly faster emptying of the manifold at increasingly fast engine speed, this becomes clear when studying the pressure curves. The pressure gradient clearly gets faster with a faster engine speed.

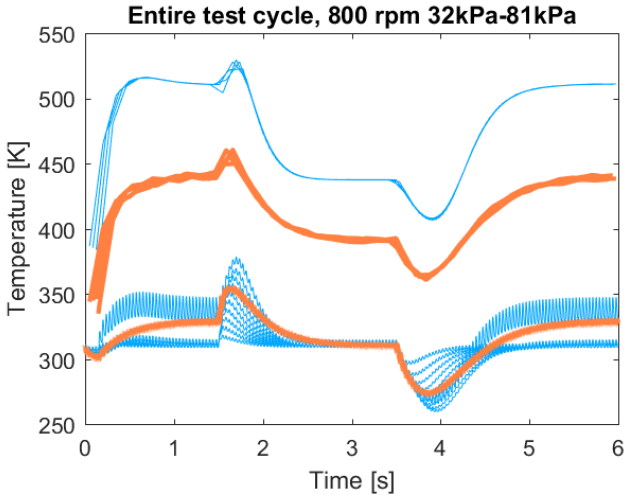

(a) Slow pressure and temperature gradient.

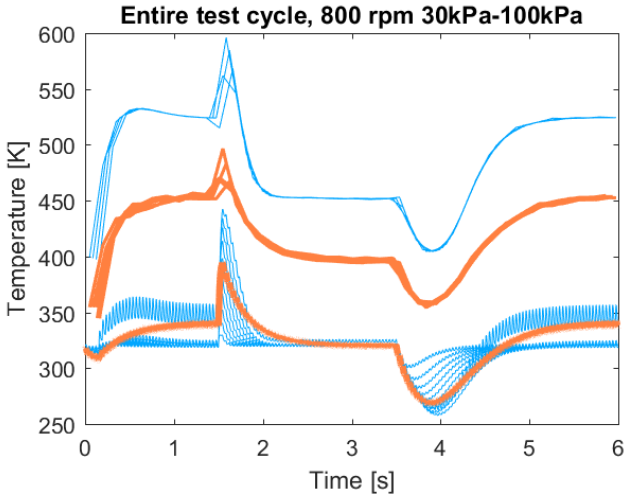

(b) Fast pressure and temperature gradient.

Figure 6.10: *Figure showing the adiabatic control volume temperature and temperature at IVC in orange and a 10 control volume implementation of Method 1 in blue. The in-cylinder temperatures are the two deviating groups of lines at a higher temperature level.*

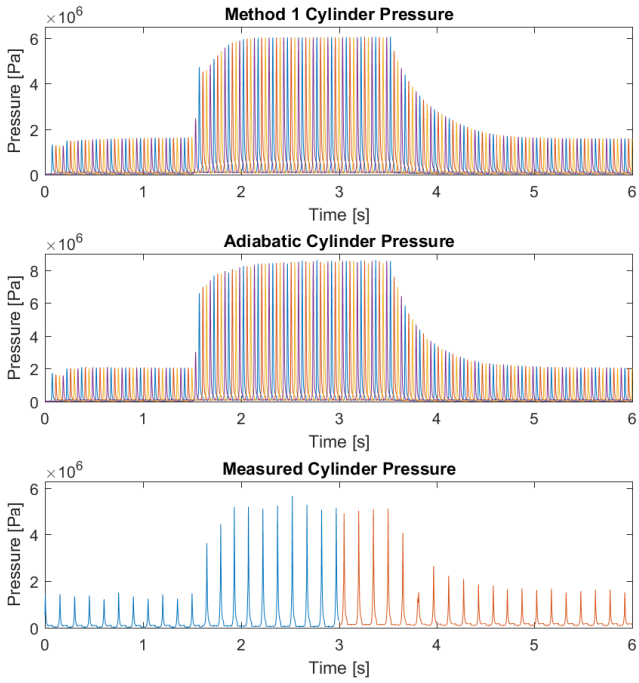

Figure 6.11: *Simulated cylinder pressures for the adiabatic model and Method 1. The measured cylinder pressure, sampled during a similar pressure transient, was done during a much longer duration, the data is therefore cut in two pieces - hence the blue and orange colored lines. Method 1 appears to be closer to the measured pressure levels than the adiabatic model.*

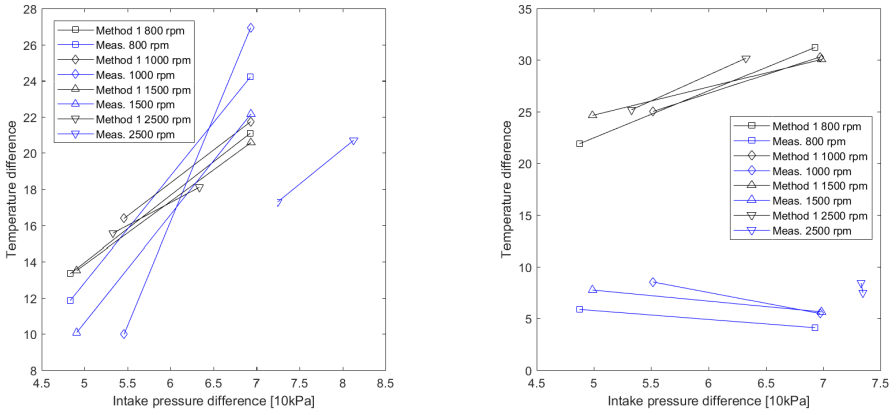

(a) Positive pressure gradient.

(b) Negative pressure gradient.

Figure 6.12: *Pressure difference and engine RPM correlation with the absolute temperature difference.*

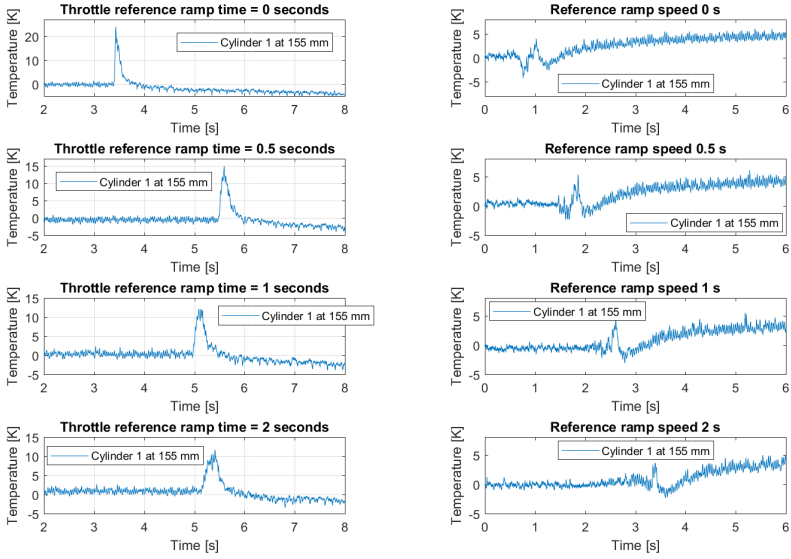

(a) Positive pressure gradient.

(b) Negative pressure gradient.

Figure 6.13: *Throttle ramping time correlation with the absolute temperature difference at 800 rpm and a throttle step from 3% to 100 %. The temperatures has been normalized in order to simplify the comparison.*

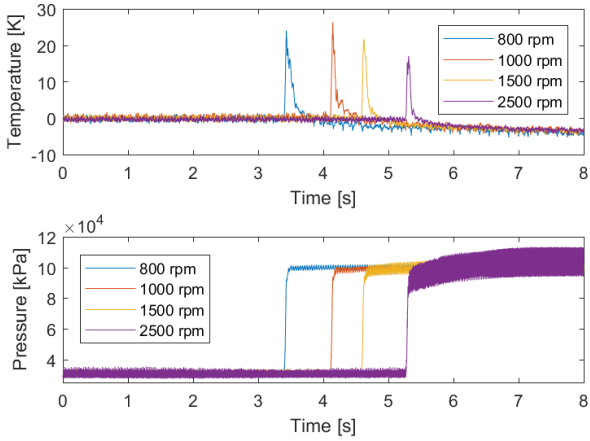

(a) Positive pressure gradient.

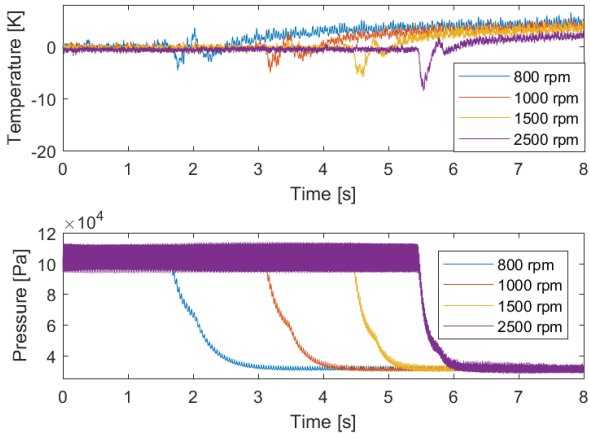

(b) Negative pressure gradient.

Figure 6.14: *Similar pressure step made for four different engine speeds; 800, 1000, 1500 and 2500 RPM. The temperatures has been normalized in order to simplify the comparison.*

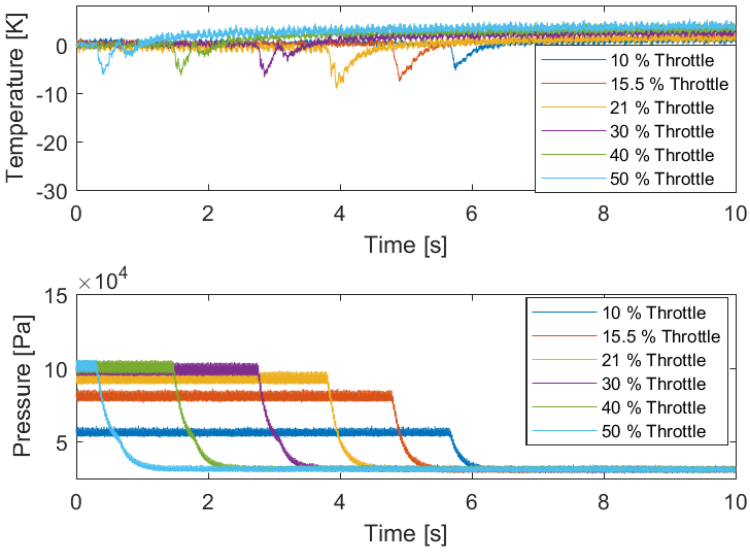

Figure 6.15: *Plot of the negative temperature transient for 6 different steps in throttle position at 1500 RPM. The throttle percentage correspond to the maximum throttle position, this renders in different maximum pressures. The theoretical trend for the negative transient is intact up until a step size corresponding to a 31% throttle opening. The temperature transients beyond 31 % are of similar magnitude and increases the temperature in an abnormal way. The pressure gradient is also impacted as it get a momentary slightly less negative gradient which looks like a dent in its curve.*

6.3.2 Negative Transient Phenomena

The negative transients behaves, as stated previously, in a way that seems unpredictable. Figure 6.15 shows the negative transients for four different pressure (throttle) steps. The modeled theoretical trend is intact for throttle steps up until a pressure step corresponding to 30 % throttle. At 30 % throttle the current models start to lack information since the transients behave different from expected.

6.3.3 VVT-settings

The VVT-settings, i.e. settings regarding the gap between the intake and exhaust valve openings, is changed for the intake and exhaust valves separately. The intake valve settings are changed in Figure 6.16 and the exhaust valve settings are changed in Figure 6.17. The figures shows the temperature measured at 130 mm in cylinder four. The stationary temperatures at low pressure, i.e before the first spike and after the second, gets higher for a higher phase shift in both cases.

The positive and negative transients shows similar behaviours as during default VVT-settings; the positive transient has a clear spike and the negative transient is clearly smaller or nonexistent. Transient temperatures at 155 mm showed no clear trend regarding the maximum temperature transients. The stationary levels which might look as they get progressively more affected by measurement noise are probably impacted by an increased amount of backflow. A backflow would cause a noise-alike temperature measurement and increase the stationary levels. Figure 6.18 shows the positive transients in detail, the pulsation phase shift between the measurements from cylinder three and four during the low intake pressure phase supports the hypothesis of backflow as well as the amount of pulsations – which matches with the engine speed of 1000 RPM. The pulsations during high intake pressure (after the temperature transient) shows a potential flow from the intake directly to the exhaust manifold, this is extra pronounced in cylinder four. The direction of the VVT phase shift shows a clear connection to the magnitude of the pulsations at low intake pressure, as a 30 CA phase shift for the intake valves moves the opening into a compression stoke of the cylinder. This means that the cylinder pushes residual gases and exhaust gas into the intake manifold. Whereas the phase-shifted exhaust camshaft is shifted further into the intake-stroke, which means that the cylinder's working against a backflow effect. This effect is not tested for the simulation case as its current fuel controller cannot approximate the residual gas when there is an overlap between the intake and exhaust valves.

6.3.4 Turbo-boosted Pressure Transient

Figure 6.19 shows how a pressure gradient mainly caused by the turbo increasing the mass flow via the compressor. The positive pressure gradient is clearly slower which, as concluded before, results in a lower temperature transient. The temperature after the initial pressure gradient increases slowly until the negative pressure transient is executed. The negative pressure transient is much faster which consequently resulted in a bigger negative temperature transient.

6.4 Sensitivity Analysis

A sensitivity analysis is presented in Table 6.9. The sensitivity analysis induces an isolated proportional model error in the cylinder temperature and pressure. It varies the amount of control volumes representing the 1-D interpreted intake manifold. The throttle and intake manifold mass flows are tested at a 'worst case'-scenario. The 'worst case'-scenario represents two cases, either an over-estimation before the pressure step and under-estimation during the higher pressure, or an under-estimation before the step and and over-estimation during the higher pressure. These scenarios will vary the pressure difference between a broad set of intervals. The transient temperatures at the corresponding control volumes are compared to the measured temperature and is presented with its RMSE, maximum temperature deviation and maximum/minimum in-cylinder

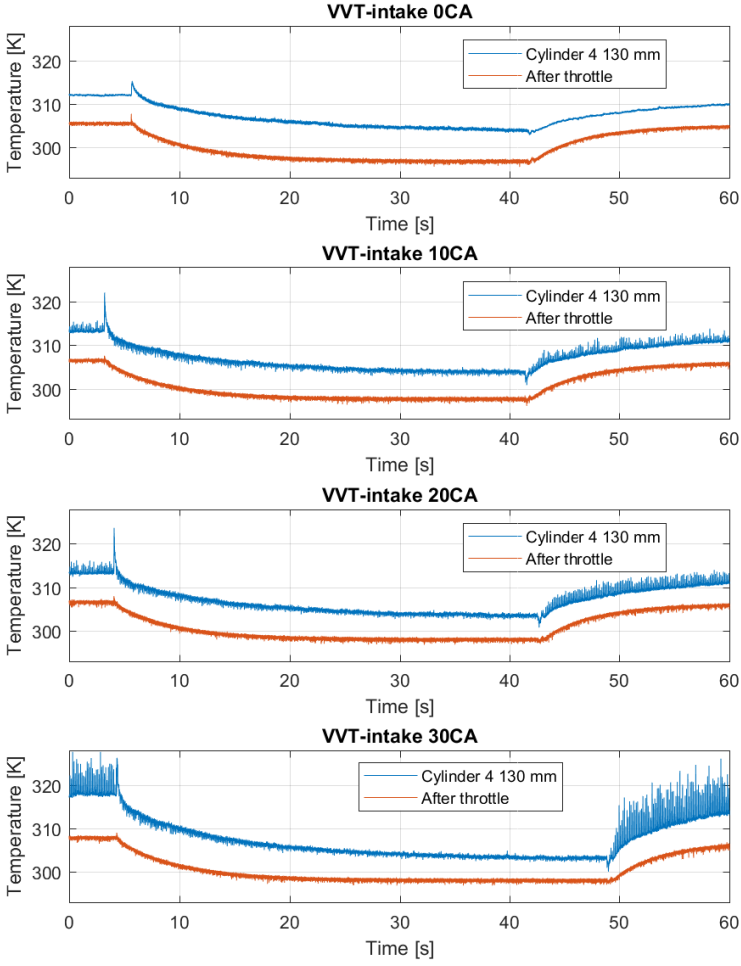

Figure 6.16: *VVTi settings changed at 1000 RPM and 30kPa-100kPa. The orange line represents the temperature directly after the throttle. The exhaust cam axle is not phase shifted.*

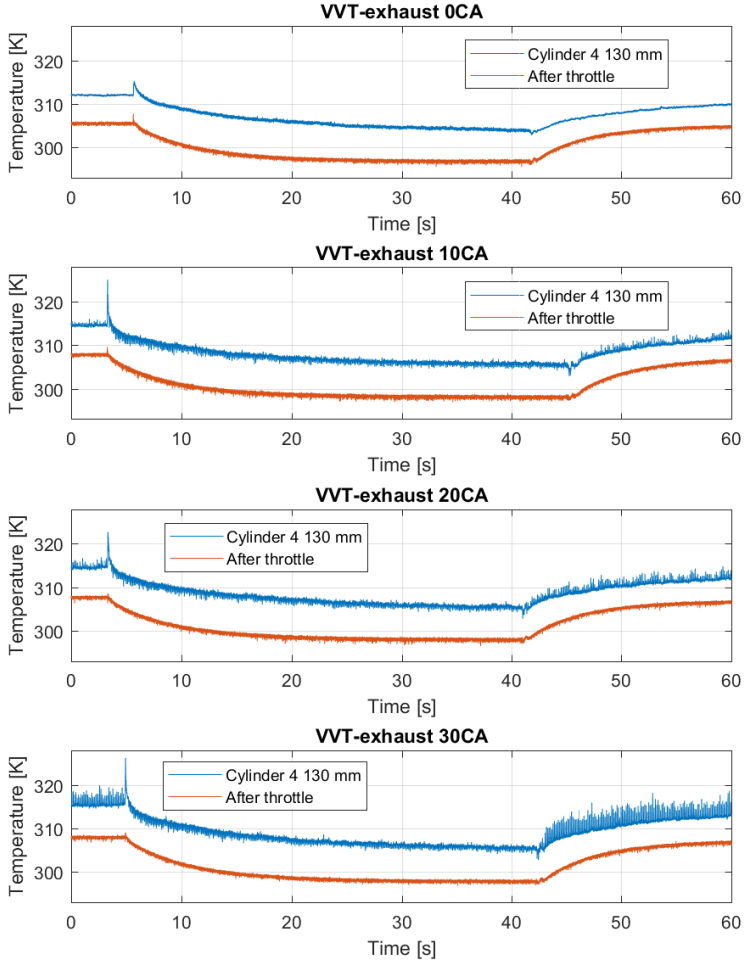

Figure 6.17: *VVTe settings changed at 1000 RPM and 30kPa-100kPa. The orange line represents the temperature directly after the throttle. The intake cam axle is not phase shifted.*

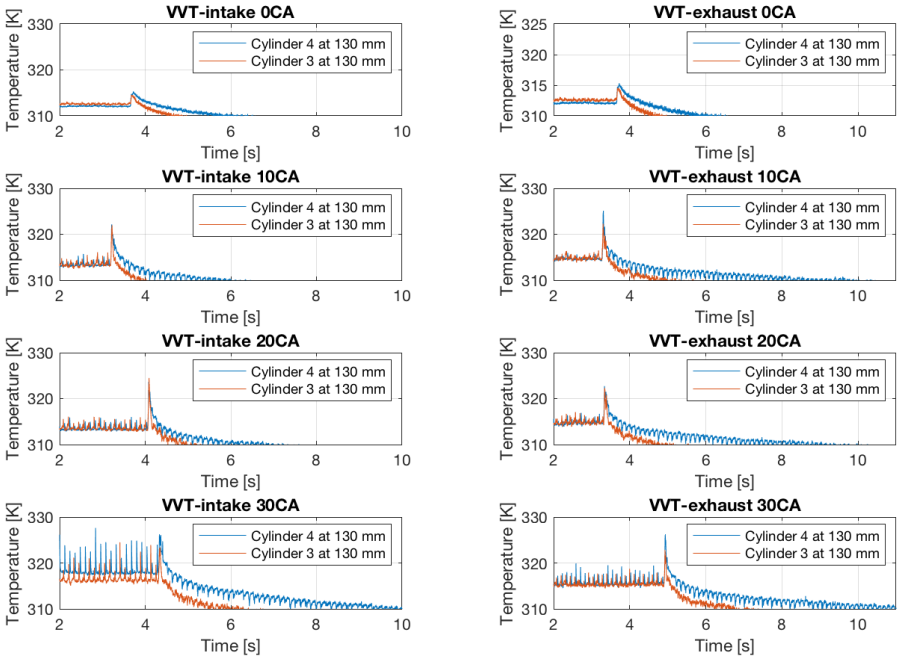

(a) Intake VVT crank angle changed.

(b) Exhaust VVT crank angle changed.

Figure 6.18: *Magnified picture of the temperature measurements at cylinder three and four at 130 mm during varied VVT settings.*

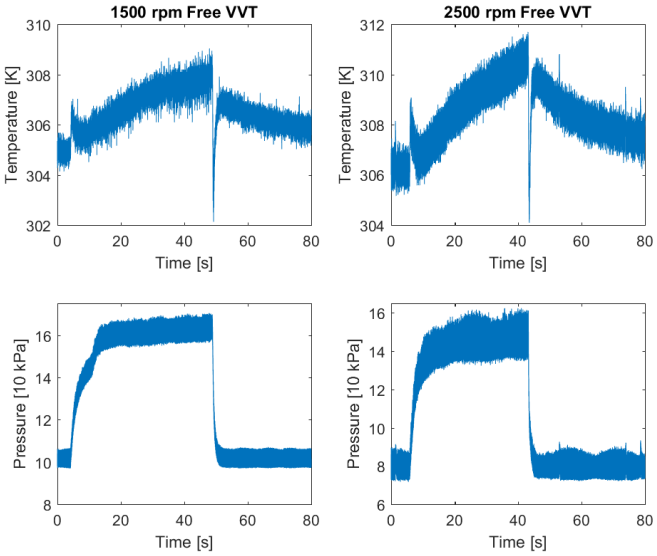

Figure 6.19: *Pressure gradient mainly powered by the turbo tested at 1500 RPM and 2500 RPM. The turbo primarily boosts the intake pressure above atmospheric pressure (i.e. above 100 kPa).*

temperature at IVC. This captures the accuracy of the model and how the maximum temperatures, both at the approximated sensor position and in-cylinder, changes. Table 6.10 shows a smaller sensitivity analysis regarding the approximated length of the intake manifold. All lengths are changed uniformly which means that the sensor is assumed to be placed in the same corresponding control volume, all volumes are kept constant.

Table 6.9: *Sensitivity analysis varying the throttle mass flow, intake valve mass flow, cylinder temperature, cylinder pressure and amount of control volumes representing the 1-D interpretation of the intake manifold. The sensitivity analysis is divided into two parts; one for the positive transient and one for the negative transient.*

Positive tr.		-10/+10 %	-5/+5 %	-2/+2 %	Reference	+2/-2 %	+5/-5 %	+10/-10 %
Throttle	RMSE	3.57	3.36	3.238	3.15	3.07	2.91	2.68
	Max dev.	2.29 %	2.12 %	2.02 %	1.95 %	1.86 %	1.73 %	1.51 %
	T_{IVC}	552 K	545.8 K	542.3 K	540 K	538.4 K	534.9 K	530 K
Intake Valve	RMSE	3.153	3.1541	3.155	3.1527	3.1562	3.157	3.116
	Max dev.	1.935 %	1.94 %	1.941 %	1.945 %	1.944 %	1.948 %	1.954 %
	T_{IVC}	539.9 K	540.03 K	540.12 K	540.05 K	539.95 K	540.44 K	540.26 K
		-20 %	-15 %	-5 %	Reference	+5 %	+15 %	+20 %
Cyl. Temp.	RMSE	3.143	3.146	3.15	3.153	3.1524	3.15	3.149
	Max dev.	1.94 %	1.9459 %	1.9457 %	1.95 %	1.945 %	1.942 %	1.940 %
	T_{IVC}	443.1 K	468.48 K	516.9 K	540 K	562.77 K	606.65 K	627.4 K
Cyl. Press.	RMSE	2.91	2.95	3.07	3.15	3.23	3.37	3.44
	Max dev.	1.951 %	1.958 %	1.952 %	1.95 %	1.932 %	1.9 %	1.88 %
	T_{IVC}	548 K	546.37 K	541.98 K	540 K	538.7 K	536.05 K	534 K
		2	5	8	Reference	12	15	18
Control Volume	RMSE	13.46	3.25	5	3.15	5.22	3.29	3.83
	Max dev.	6 %	1.77 %	2.88 %	1.95 %	3.21 %	2.17 %	2.48 %
	T_{IVC}	489 K	522.33 K	535.4 K	540 K	543.9 K	547.8 K	549.74 K
Negative tr.		-10/+10 %	-5/+5 %	-2/+2 %	Reference	+2/-2 %	+5/-5 %	+10/-10 %
Throttle	RMSE	7.97	7.25	6.84	6.57	6.32	5.96	5.37
	Max dev.	7.15 %	6.53 %	6.17 %	5.92 %	5.69 %	5.37 %	4.81 %
	T_{IVC}	395.4 K	396.6 K	397.6 K	398 K	399.2 K	400.27 K	402.4 K
Intake Valve	RMSE	6.6	6.59	6.558	6.576	6.58	5.57	6.562
	Max dev.	5.949 %	5.939 %	5.935 %	5.921 %	5.929 %	5.92 %	5.909 %
	T_{IVC}	398.3 K	398.36 K	398.36 K	398.43 K	398.3 K	398.53 K	398.51 K
		-20 %	-15 %	-5 %	Reference	+5 %	+15 %	+20 %
Cyl. Temp.	RMSE	6.62	6.6	6.584	6.576	6.568	6.55	6.55
	Max dev.	5.964 %	5.95 %	5.928 %	5.92 %	5.913 %	5.904 %	5.901 %
	T_{IVC}	329.93 K	348.6 K	382.5 K	398 K	413.6 K	441.7 K	454.78 K
Cyl. Press.	RMSE	7.11	7.00	6.73	6.57	6.41	6.05	5.86
	Max dev.	6.78 %	6.52 %	6.08 %	5.92 %	5.78 %	5.49 %	5.32 %
	T_{IVC}	406.2 K	403.37 K	399.63 K	398 K	397.26 K	396.27 K	396 K
		2 CV	5 CV	8 CV	Reference	12 CV	15 CV	18 CV
Control Volume	RMSE	14.85	6.66	8.18	6.57	8.35	6.72	7.3
	Max dev.	10.38 %	5.95 %	7.27 %	5.92 %	7.56 %	6.2 %	6.76 %
	T_{IVC}	357.33 K	381.95 K	395.48 K	398 K	400.13 K	402.34 K	403.23 K

Table 6.10: *Sensitivity analysis varying the intake manifold length. All length dimension are changed uniformly. Therefore is the sensor placement assumed to be constant.*

Positive tr.		-10 %	Reference	+10 %
Intake Length	RMSE	3.157	3.1527	3.1525
	Max dev.	1.939 %	1.945 %	1.946 %
	T_{IVC}	541.4 K	540.05 K	539.02 K
Negative tr.		-10 %	Reference	+10 %
Intake Length	RMSE	6.557	6.57	6.58
	Max dev.	5.91 %	5.92 %	5.935 %
	T_{IVC}	400.47 K	398 K	397.95 K

7

Discussion

This chapter presents a discussion regarding the results, proposed focus areas in order to simplify current models and current uncertainties that lies within the implemented models and measurements.

7.1 Simulation Models

This section discusses the results presented regarding the choice, setup and validation of the intake manifold models.

7.1.1 Model Choice

Table 6.1 showed the step requirements for each method. These requirements are hefty compared to the 0-D adiabatic control volume model presented in Section 4.1.3 which can be implemented without any stability requirements (without the CFL criterion), the engineer merely sets the time step according to his/her performance specification. It is apparent that *Method 2* has too complex plug-volumes. *Method 1 & 3* has similar requirements but *Method 1* seems to behave a bit more logical during the end of the transient, as the temperature of the first control volume does not go below the ambient temperature - which would be logical if we had a negative gradient on the pressure, but that is not the case. *Method 1* was therefore the preferred method and the model that was implemented as the 1-D intake manifold dynamics model for the full simulations.
The adiabatic model shows to consider a lot of the stationary backflow which is good when trying to model to model the stationary temperature. Its positive and negative transients, e.g. seen in Figure 6.10, are not quite as accurate as it models a transient temperature corresponding to an average transient temperature in the control volume, i.e. the transient temperature corresponds to the fifth control

volume in a ten control volume configuration. The adiabatic models in-cylinder temperature deviates quite much from *Method 1*s, this can be related to its cylinder pressure seen in Figure 6.11. It is the assumed lower intake temperature that increases the modeled cylinder pressure as a higher mass of air fills the cylinder. The residual gas fraction is reduced as a consequence of a higher cylinder pressure at EVO which increases the exhaust valve mass flow. The generally higher amount of mass in the cylinder also decreases the temperature, which is why the adiabatic model deviates at the stationary levels. In order to get a correct cylinder temperature, some model that corrects the cylinder pressure is needed, i.e. the presented in-cylinder temperature for the adiabatic model can be assumed to be misleading. But its not a far fetched assumption since its cylinder pressure is significantly higher than the measured cylinder pressure, while *Method 1* is fairly close to the measured pressure.

Method 1 seems to capture most of the aspects affecting the positive transient, such as the pressure difference, pressure step time constant and engine speed, as its validations were quite consistent through all operating conditions which tested all of these. Though smaller and slower pressure steps has a clear tendency towards over-estimation. A possible explanation to this over-estimation could be that the current implementation of volumetric efficiency (intake valve discharge coeffcients) is closer to the actual volumetric efficiency of the intake manifold at higher throttle mass flows than lower. It could also be coupled to the placement of the sensor - which is in a curvature, the pressure gradient in a curvature is usually over-estimated according to Renberg (2008). The over-estimated pressure gradient leads to an increased temperature transient.

If an implementation using current models is desired, one would get better results not trying to predict the negative transient – when concluding from the validation data. This statement might be untrue as what's happening beyond the validation point is unknown. A possible explanation to this phenomena could be that it is coupled to delayed ignitions and inefficient combustions resulting in extra high cylinder temperatures. A higher cylinder temperatures combined with what seems like higher backflows than modeled would yield in a similar effect.

7.1.2 Control Volume Setup

The length of the intake system was quite hard to approximate from two standpoints. The first being the fact that the flow does not flow in a single direction, it enters from the bottom and turns 90 °into the pipes and then into the engine. The ideal case would be that the in and out flow of the control volume was separated into two end-points. The other obstacle was the lack of hard measurement information, some measurements has been done by hand and is therefore due to some margin of error. The sensitivity analysis, in Table 6.10 shows that the length has little impact on the actual end result, i.e. the in-cylinder temperature at IVC, but a major impact when validating a specific point (as the RMSE is increased quite a lot at +10 %). But as the maximum deviation is remained quite constant one can conclude that a changed cross-sectional area mostly impacts the length and propagation of the transient.

Inspecting the simulation criterion presented by Courant et al. (1928) (see Eq. (4.21)) one can see that the length and cross sectional area impacts the approximated required time step - thus making the length a tuning parameter between accuracy and simulation time as it also changes to cross sectional area. A smaller cross sectional area would decrease the required time step.

The amount of control volumes implemented depends on accuracy and computational requirements. The sensitivity analysis in Table 6.9 shows that the in-cylinder temperature is increased with a finer control volume discretization. The positive and negative transient in-cylinder temperature difference, between five and 18 control volumes is only about 5 %, therefore a substantial cut in computational cost can be made at a model-to-model relative decrease in accuracy at 5 %. The ability to validate at this specific sensor placement varies with how the sensor is placed relative to the control volumes, but the general accuracy (above two control volumes) is somewhat constant.

7.1.3 Non-intake manifold model Accuracy Requirements

Model accuracy dependency was investigated by inducing varying percentages of model errors on the throttle and intake mass flow, cylinder pressure and temperature, see Table 6.9. Inducing a modeling error for the throttle and intake valves would impact the mass balance which basically changes the pressure dynamics, a lower throttle mass flow equals a lower intake pressure which in turn equals a lower transient temperature. A throttle mass flow model error clearly impacts the end result, as both the validation point and in-cylinder temperatures are impacted during both transients. The validation point temperature changes as the pressure dynamics changes, thus varying the model validation accuracy. The in-cylinder temperature is impacted by two effects – both by a higher/lower maximum temperature transient and by a higher/lower intake pressure that changes the cylinder mass flow. As an example at -10%/+10% where the maximum transient temperature is higher as the pressure step is increased and the cylinder is filled with more of the hotter transient temperature as the intake pressure is higher.

The importance of the intake valve mass flow is noticeably lower, as both the temperature at the validation point as well as in-cylinder temperatures remains close to unchanged. As the intake valve mass flow relates to the model often referred to as volumetric efficiency, which often is mapped for the specific intake manifolds and operating points. A similar approach for the intake valve discharge coefficients would increase the model accuracy but not significantly. A mapped intake valve discharge coefficient and throttle would not impact the temperature much to these matched/iterated pressure curves, i.e. the throttle opening area is not the same in simulation as in the experiment. But a mapped intake valve dynamics and a better throttle model would reduce total simulation time.

The in-cylinder models proves to be somewhat more important. An overestimation of the cylinder pressure leads to a lower amount of residual gas which in the end changes the cylinder pressure at IVO which changes the intake valve

mass flow. The combined effect means that the in-cylinder temperature at IVC is decreased by an increased intake valve mass flow and a decreased amount of residual gas. The cylinder temperature increases or decreases the temperature of the backflow and thus has the main impact on the stationary levels during low intake manifold pressure. The in-cylinder temperature at IVC and temperature of the residual gas would be inherently majorly impacted. The cylinder temperature is therefore incredibly important. The VVT-settings also impacts the in-cylinder temperature as it adjusts the residual gas fraction.

7.2 Intake Temperature Model Simplification

The results shows that there are several key areas that affects the *transient* intake temperature. Key areas during a *positive transient* are

- Pressure difference
- Pressure step time constant
- Engine speed

and key areas during a *negative transient* are as follows.

- Pressure difference
- Pressure step time constant
- Engine speed
- Backflow
- *Undefined* coupled to the negative transient phenomena

An idea to rationalize is to include the effect from pressure difference and time constant by either modeling the pressure gradient, or by using estimated mass flows, or by measuring the pressure and calculating the gradient. Solely the positive intake manifold temperature transient is not very dependent on the residual gas composition nor the backflow (also coupled to VVT-settings) since both of their effects decreases with the increased intake manifold pressure. Their effects are therefore more important during the negative transient as the intake manifold pressure decreases.

Another idea to approximate only the transient temperatures would be to use the heat transfer term in the adiabatic control volume to manipulate the otherwise 0-D output into a 1-D output. The idea is to map the heat transfer term to give different outputs depending on the manifold position. It would basically mean a higher heat transfer term further into the manifold. The mapping could either be done from measurements or simulations. The map should be paired with some kind of trigonometric function, as a sinus, cosinus or Vibe function. Stationary temperatures has to be approximated by some other method as stationary temperatures, especially further into the manifold, is particularly dependent on the intake pressure (backflow), i.e. a trigonometric model would not be suitable for a stationary scenario as it induces a stationary temperature offset.

7.3 Measurement uncertainties

The sensors placed at 130 mm in both cylinder three and four shows generally higher stationary temperatures, which is reasonable as they are placed further inside the manifold. The temperature further into the manifold should be hotter as the air gets further affection from heat transfer and potential backflow. But the transient temperatures, which is shown in Figure 6.16 and 6.17 at 0 CA phase-shifted VVT-settings (<5 K difference) compared with the transient temperatures shown in Figure 6.6b (>20 K difference) are clearly lower. This seems unreasonable and is probably due to a too low mass flow hitting the sensor (since the sensor is not placed entiery perpendicular to the flow).
The transient temperature measurements may also be influenced by the intake valve opening of the individual cylinders, i.e. the peak transient temperature measured at cylinder one will be decreased if the intake valves at cylinder one is opened slightly before the peak temperature.

8

Conclusions & Future Work

This chapter will summarize some conclusions and suggest relevant areas for future work.

8.1 Conclusions

Conclusions based on the results and discussion are listed below.

- *Method 1* appeared to be the most efficient 1-D model among the tested methods. Current implementation has higher accuracy for higher throttle mass flows.
- An implementation with more than five representative control volumes is a choice that has to be motivated with a trade-off between accuracy and computational cost, where accuracy has a high computational cost.
- There are four main areas which affects the transient temperatures; the pressure difference, pressure step time constant, engine speed and backflow. Backflow has biggest impact during low intake pressure, i.e. during a negative transient or during low intake pressure stationary conditions.
- Turbo control has little impact on the transient temperatures, it does however generally increase the intake air temperature.
- VVT-control has little impact on transient temperatures at the more reliable 155 mm sensor position.
- Current simulation models lacks information in order to accurately model the negative transients.

8.2 Future Work

A list of potential areas for improvement and further development.

- Use the complete comprehension retrieved in the air-path simulation model and presented simplification ideas as resource when simplifying the transient temperature model. This is a logical step towards making the model implementable in current ECUs.
- Redo measurements logged in-sync with the crank angle. This would help when trying to conclude if the transient timing was amplifying or reducing the transient temperature. Redo measurements with the sensors further into the pipes. This would expand the validated section and therefore reduce the temperature ”grey area”.
- Use measured data in the simulation, such as the cylinder pressures instead of simulating the combustion. This comes with the known complexity of pegging the cylinder pressure, but would nonetheless significantly reduce the required computational power and provide intake valve mass flows. One could also install slower temperature sensors at different positions in the manifold and utilize sensor fusion to adjust the stationary levels and maintain the modeled transient behaviour. Similar sensor fusion could be done with a pressure sensor that calibrates the mass flow estimations.
- Improve the combustion model - add heat transfer and a Vibe-parameter predictor. A Vibe-parameter predictor is presented in Thornberg and Eriksson Kraft (2018). This is important as the cylinder temperature proved to be very important when estimating the in-cylinder temperature at IVC.
- Improve throttle and intake valve model. This would improve model accuracy, a plausible major improvement for slow transients.
- Investigate the transient (and stationary) temperature difference between the individual cylinders. The two inner cylinders gets a bigger portion of fresh air than the two outer cylinders. Thus making the assumption of a straight pipe to all cylinders invalid.
- Only negative overlap has been simulated, a new fuel controller that enables further simulations with different VVT-settings would be interesting for further understanding of the in-cylinder temperature. The new fuel controller could use more advanced residual gas fraction methods or simply ignore the residual gas – the analysis could then be focused on the cylinder pressure and temperature and the effect it has on the in-cylinder temperature at IVC.
- Investigate or implement heat transfer models. All models are heat transfer compatible as a heat transfer term is implemented for each control volume.

Appendix

A

Test list

This appendix presents a complete test list. This appendix is reffered to in Section 5.4

- LVVT = Locked VVT @ negative 8.6° overlap.
- FVVT = Free VVT control, i.e. volvo ECU-controlled.
- CVVT = Changed VVT settings.

Table A.1: *LVVT 800 rpm.*

Test	RPM	Step	Ramp time
1	800	3-13%	0
2	800	3-21%	0
3	800	3-22%	0
4	800	3-23%	0
5	800	3-25%	0
6	800	3-30%	0
7	800	4-40%	0
8	800	3-50%	0
9	800	3-60%	0
10	800	3-80%	0
11	800	3-100%	0

Table A.2: *LVVT 1000 rpm.*

Test	RPM	Step	Ramp time
12	1000	3.5-13%	0
13	1000	3.5-21%	0
14	1000	3.5-22%	0
15	1000	3.5-23%	0
16	1000	3.5-25%	0
17	1000	3.5-30%	0
18	1000	3.5-40%	0
19	1000	3.5-50%	0
20	1000	3.5-60%	0
21	1000	3.5-80%	0
22	1000	3.5-100%	0

Table A.3: *LVVT 1500 rpm.*

Test	RPM	Step	Ramp time
23	1500	5.5-13%	0
24	1500	5.5-21%	0
25	1500	5.5-22%	0
26	1500	5.5-23%	0
27	1500	5.5-25%	0
28	1500	5.5-30%	0
29	1500	5.5-40%	0
30	1500	5.5-50%	0
31	1500	5.5-60%	0
32	1500	5.5-80%	0
33	1500	5.5-100%	0

Table A.4: *LVVT 2500 rpm.*

Test	RPM	Step	Ramp time
34	2500	8.5-50%	0
35	2500	8.5-100%	0

Table A.5: *LVVT 800 rpm.*

Test	RPM	Step	Ramp time
36	800	3-100%	0.5
37	800	3-100%	1
38	800	3-100%	1.5
39	800	3-100%	2

Table A.6: *LVVT 800 and 1000 rpm.*

Test	RPM	Step	Ramp time
40	800	30-45kPa	0
42	800	30-45kPa	0.5
44	800	30-45kPa	1
46	1000	30-45kPa	0
48	1000	30-45kPa	0.5
50	1000	30-45kPa	1

Table A.7: *LVVT 800 rpm.*

Test	RPM	Step	Ramp time
52	800	3-10%	0
53	800	3-17%	0
54	800	3-19%	0

Table A.8: *LVVT 1000 rpm.*

Test	RPM	Step	Ramp time
55	1000	3.5-10%	0
56	1000	3.5-16%	0
57	1000	3.5-19%	0

Table A.9: *LVVT 1500 rpm.*

Test	RPM	Step	Ramp time
58	1500	5.5-10%	0
59	1500	5.5-15.5%	0
60	1500	5.5-20%	0
61	1500	5.5-35%	0
62	1500	5.5-36%	0
63	1500	5.5-37%	0
64	1500	5.5-38%	0

Table A.10: *FVVT 800, 1000, 1500 and 2500 rpm.*

Test	RPM	Step	Ramp time
65	800	3-10%	0
66	800	3-13%	0
67	800	3-25%	0
68	800	3-50%	0
69	800	3-60%	0
70	800	3-100%	0
71	1000	3.5-11..6%	0
72	1000	3.5-16%	0
73	1000	3.5-25%	0
74	1000	3.5-50%	0
75	1000	3.5-60%	0
76	1000	3.5-100%	0
77	1500	5.5-10%	0
78	1500	5.5-15.5%	0
79	1500	5.5-20%	0
80	1500	5.5-25%	0
81	1500	5.5-35%	0
82	1500	5.5-38%	0
83	1500	5.5-50%	0
84	1500	5.5-100%	0
85	2500	8.5-50%	0
86	2500	8.5-100%	0

Table A.11: *CVVT 1000 and 2500 rpm.*

Test	RPM	Step	Ramp time	VVTi	VVTe
87	1000	3.5-100%	0	0	10
88	1000	3.3-100%	0	0	20
89	1000	2.89-100%	0	0	30
90	1000	3.75-100%	0	10	0
91	1000	3.89-100%	0	20	0
92	1000	3.75-100%	0	30	0
93	2500	8.5-100%	0	0	10
94	2500	8.2-100%	0	0	20
95	2500	7.8-100%	0	0	30
96	2500	8.7-100%	0	10	0
98	2500	8.9-100%	0	30	0
999	2500	8.5-100%	0	30	10
1000	2500	8.5-24.2	0	0	5
1001	2500	8.5-24.3	0	0	9
1002	2500	8.378-24	0	0	15

Table A.12: *Turbo steps at 1500 and 2500 rpm. FVVT was activated. Version 1 is step from minimum throttle to a much higher throttle position with closed wastegate. Version 2 is a step in wastegate position (from open to closed) at a throttle position that permits turbocharging.*

Test	RPM	Version
103	1500	1
104	1500	2
105	2500	1
106	2500	2

Bibliography

P. Astrid. Reduction of process simulation models : a proper orthogonal decomposition approach. *Eindhoven: Technische Universiteit Eindhoven, DOI: 10.6100/IR581728*, 2004. PhD Thesis. Cited on page 11.

S.H. Baik and K.M. Chun. A study on the transient knock control in a spark-ignition engine. *SAE International 981062 ISSN 0148-7191*, 1996. URL https://saemobilus.sae.org/content/981062/. Cited on page 9.

W. Bauer and J.B. Heywood. Flow characteristics in intake port of spark ignition engine investigated by cfd and transient gas temperature measurement. *SAE Technical Paper 961997, doi:10.4271/961997.*, 1996. URL https://saemobilus.sae.org/content/961997/. Cited on page 10.

W. Bauer, P. Balun, and J.B. Heywood. Heat transfer and mixture vaporization in intake port of spark-ignition engine. *SAE Technical Paper 972983, doi:10.4271/972983*, 1997. URL https://saemobilus.sae.org/content/972983/. Cited on page 11.

B.A. Befrui. Cfd simulation and comparison with measurement of steady flow in intake ports and combustion chambers. 1994. URL https://www.researchgate.net/publication/299978552_CFD_Simulation_and_Comparison_with_Measurement_of_Steady_Flow_in_Intake_Ports_and_Combustion_Chambers. Cited on page 10.

D. Blomqvist, S. Byttner, U. Holmberg, and T. Rögnvaldsson. Different strategies for transient control of the air-fuel ratio in a SI engine. oct 2000. ISSN 0148-7191. doi: https://doi.org/10.4271/2000-01-2835. URL https://doi.org/10.4271/2000-01-2835. SAE Technical Paper 2000-01-2835. Cited on page 10.

J. Bohbot, D. Klahr, M. Zolver, and A. Torres. A three dimensional modelling of combustion in a direct injection diesel engine using a new unstructured parallel solver. *International Conference on Computational Science and its Applications, proceedings pp483-492, ISSN: 0302-9743 Online ISSN: 1611-3349*, 2003. Cited on page 11.

C-O Cheng, W.K. Cheng, and J.B. Heywood. Intake port phenomena in a spark-ignition engine-at part load. *SAE Technical Paper 912401, doi:10.4271/912401.*, 1991. URL https://saemobilus.sae.org/content/912401/. Cited on page 10.

R. Courant, K. Friedrichs, and H. Lewy. Über die partiellen differenzengleichungen der mathematischen physik. *Mathematische Annalen*, 100(1):32–74, Dec 1928. ISSN 1432-1807. doi: 10.1007/BF01448839. URL https://doi.org/10.1007/BF01448839. Cited on pages 11, 19, 37, and 59.

J. Crank and P. Nicolson. A practical method for numerical evaluation of solutions of partial differential equations of the heat-conduction type. *Baltzer Science Publishers, Baarn/Kluwer Academic Publishers*, 1996 (original: 1947). URL https://doi-org.e.bibl.liu.se/10.1007/BF02127704. Cited on page 11.

A. Douaud and P. Eyzat. Four-octane-number method for predicting the anti-knock behavior of fuels and engines. *SAE Technical Paper 780080, doi:10.4271/780080.*, 1978. URL https://saemobilus.sae.org/content/780080. Cited on page 9.

L. Eriksson. Spark advance for optimal eficiency. *SAE International 1999-01-0548 ISSN 0148-7191*, 1999. URL https://saemobilus.sae.org/content/1999-01-0548/. Cited on page 9.

L. Eriksson and I. Andersson. An analytic model for cylinder pressure in a four stroke SI engine. mar 2002. ISSN 0148-7191. doi: https://doi.org/10.4271/2002-01-0371. URL https://doi.org/10.4271/2002-01-0371. Cited on page 21.

L. Eriksson and L. Nielsen. Modeling and control of engines and drivelines. *John Wiley Sons Ltd, ISBN:9781118479995*, 2014. Cited on pages 6, 7, 11, 12, 20, and 22.

L. Eriksson and A. Thomasson. Cylinder state estimation from measured cylinder pressure traces - a survey. *IFAC-PapersOnLine, Elsevier, ISSN: 2405-8963*, 2017. URL https://doi.org/10.1016/j.ifacol.2017.08.2483. Cited on page 10.

JA Gatowski, En N Balles, KM Chun, FE Nelson, JA Ekchian, and John B Heywood. Heat release analysis of engine pressure data. 1984. SAE Technical paper 841359. Cited on page 23.

M. Haletad, L.J. Kirsch, A. Prothero, and C.P. Quinn. A mathematical model for hydrocarbon autoignition at high pressures. *Royal Society Journal Article*, 346 (1647):515–538, 1975. URL http://www.jstor.org.e.bibl.liu.se/stable/78834. Cited on page 9.

Yun Y. Ham, Kwang M. Chun, Jae H. Lee, and Kwang S. Chang. Spark-ignition engine knock control and threshold value determination. *SAE International*

960496 ISSN 0148-7191, 1996. URL https://saemobilus.sae.org/content/960496/. Cited on page 9.

Yoshisuke Hamamoto, Eiji Tomita, Masaki Yamanaka, and Motoshi Kataoka. Heat transfer to the wall of end gas side during propagation of premixed flame in a closed vessel : Heat flux measurements by both interference image analysis and thin surface thermocouple methods. *JSME International Journal Series B*, 39(4):836–843, 1996. doi: 10.1299/jsmeb.39.836. Cited on page 19.

J.B. Heywood. Internal combustion engine fundamentals. *McGraw-Hill Professional*, 1988. Cited on pages 7, 10, 11, 22, 25, and 28.

L. Hosain and R.B. Fdhila. Literature review of accelerated cfd simulation methods towards online applications. *The 7th International Conference on Applied Energy – ICAE2015, Elsevier*, 2015. URL https://doi.org/10.1016/j.egypro.2015.07.714. Cited on page 11.

M. Ichiyanagi and T. Suzuki. Implementation of air-fuel ratio feed-forward controller considering heat transfer at intake system to SI engine. *SAE Technical Paper 2015-01-1982*, 2015. URL https://doi.org/10.4271/2015-01-1982. Cited on page 10.

H. Izumi, Y. Kidani, and T. Suzuki. The effect of intake system heat transfer on air fuel ratio and fuel injection correction with intake system temperature. *SAE Technical Paper 2007-08-0545*, 2007. Cited on page 10.

S Kakac, R.K. Shah, and W. Aung. Handbook of single-phase convective heat transfer. *John Wiley & Sons*, 1987. URL https://doi.org/10.1080/07373938908916581. Cited on page 11.

L. Kangyoon, Y. Maru, and S. Myoungho. A study on pegging methods for noisy cylinder pressure signal. *Control Engineering Practice*, 16(8):922 – 929, 2008. ISSN 0967-0661. doi: https://doi.org/10.1016/j.conengprac.2007.10.007. URL http://www.sciencedirect.com/science/article/pii/S096706610700189X. Special Section: IFAC Conference on Analysis and Design of Hybrid Systems (ADHS'06). Cited on page 33.

M. Klein. *Single-Zone Cylinder Pressure Modeling and Estimation for Heat Release Analysis of SI Engines*. PhD thesis, Linköpings universitet, November 2007. Cited on page 23.

T. Leroy, G. Alix, J. Chauvin, A. Duparchy, and F. Le Berr. Modeling fresh air charge and residual gas fraction on a dual independent variable valve timing si engine. *SAE Int. J. Engines 1(1):627-635*, 2009. URL https://doi.org/10.4271/2008-01-0983. Cited on page 11.

G. Montenegro, A. Della Torre, A. Onorati, R. Fairbrother, and A. Dolinar. Development and application of 3d generic cells to the acoustic modelling of exhaust systems. may 2011a. ISSN 0148-7191. doi: https://doi.org/10.4271/2011-01-1526. URL https://doi.org/10.4271/2011-01-1526. Cited on pages 14 and 16.

G. Montenegro, A. Onorati, A. Della Torre, and A.J. Torregrosa. The 3dcell approach for the acoustic modeling of after-treatment devices. *SAE International Journal of Engines*, 4(2):2519–2530, sep 2011b. doi: https://doi.org/10.4271/2011-24-0215. URL https://doi.org/10.4271/2011-24-0215. Cited on pages 14 and 16.

Sepideh Nikkar. Estimation of in-cylinder trapped gas mass and composition. (LiTH-ISY-EX–17/5073–SE), June 2017. MSc. Thesis. Cited on page 24.

L.V. Plotnikov and B.P. Zhilkin. The gas-dynamic unsteadiness effects on heat transfer in the intake and exhaust systems of piston internal combustion engines. *International Journal of Heat and Mass Transfer 115 1182-1191*, 2017. URL https://doi.org/10.1016/j.ijheatmasstransfer.2017.08.118. Cited on page 12.

Ulrica Renberg. 1d engine simulation of a turbocharged si engine with cfd computation on components. *Licentiate Thesis, Royal Institute of Technology, ISRN KTH/MMK/R-08/09-SE*, 2008. Cited on pages 11, 35, and 58.

N Shiibara, H. Nakamura, and S. Yamada. Unsteady characteristics of turbulent heat transfer in a circular pipe upon sudden acceleration and deceleration of flow. *International Journal of Heat and Mass Transfer 113 490-501*, 2017. URL https://doi.org/10.1016/j.ijheatmasstransfer.2017.05.077. Cited on page 12.

K Siokos, Z. He, and R. Prucka. Assessment of model-based knock prediction methods for spark-ignition engines. *SAE Technical Paper 2017-01-0791, doi:10.4271/2017-01-0791*, 2017. URL https://saemobilus.sae.org/content/2017-01-0791/. Cited on page 9.

S. Stockar, M. Canova, Y. Guezennec, A. Della Torre, G. Montenegro, and A. Onorati. Modeling wave action effects in internal combustion engine air path systems: comparison of numerical and system dynamics approaches. *International Journal of Engine Research*, 14(4):391–408, 2013. doi: 10.1177/1468087412455747. URL https://doi.org/10.1177/1468087412455747. Cited on pages 14, 16, 17, and 18.

Strikwerda. Finite difference schemes and partial differential equations. *Wadsworth & Brooks/Cole*, 1989. Cited on page 11.

N. Thornberg and J. Eriksson Kraft. Physically based modelling for knock prediction in si engines. (LiTH-ISY-EX–18/5136–SE), June 2018. MSc. Thesis. Cited on pages 22 and 64.

I. I Vibe and F. Meißner. *Brennverlauf und kreisprozess von verbrennungsmotoren*. Verlag Technik, 1970. Cited on page 22.

X. Wang and N. Zhang. Numerical analysis of heat transfer in pulsating turbulent flow in a pipe. *International Journal of Heat and Mass Transfer 48 3957-3970*, 2005. URL https://doi.org/10.1016/j.ijheatmasstransfer.2005.04.011. Cited on page 12.

G. Woschni. A universally applicable equation for the instantaneous heat transfer coefficient in the internal combustion engine. 1967. SAE Technical Paper 670931. Cited on page 20.

H. Zapf. Contribution to the investigation of heat transfer during charge exchange of a four-stroke diesel engine. *MTZ 30*, 12, 1969. Cited on page 11.

M. Zolver, D. Klahr, J. Bohbot, and A. Toores. Reactive cfd in engines with a new unstructured parallel solver. *Oil & Gas Science and Technology - Rev. IFP*, 58(pp33-46), 2003a. URL `https://doi.org/10.2516/ogst:2003003`. Cited on page 11.

M. Zolver, D. Klahr, J. Bohbot, and A. Toores. An unstructured parallel solver for multi-phase and reactive flows in internal combustion engines. *Parallel Computational Fluid Dynamics, doi: 10.1016/B978-044451612-1/50032-9*, (pp251-258), 2003b. Cited on page 11.

P. Öberg. A dae formulation for multi-zone thermodynamic models and its application to cvcp engines. *Linköping Studies in Science and Technology Dissertation No. 1257, ISBN 978-91-7393-607-1, ISSN 0345-7524*, 2009. Cited on pages 14 and 16.